A systems view of spliceosomal assembly and branchpoints with iCLIP

Michael Briese[1,2]*, Nejc Haberman[3,4]*, Christopher R. Sibley[1,4,5]*, Anob M. Chakrabarti[3,9], Zhen Wang[1], Julian König[1,6], David Perera[7], Vihandha O. Wickramasinghe[7,8], Ashok R. Venkitaraman[7], Nicholas M. Luscombe[3,9,10], Christopher W. Smith[11], Tomaž Curk[12], Jernej Ule[1,3,4§]

[1]MRC Laboratory of Molecular Biology, Francis Crick Avenue, Cambridge, CB2 0QH, UK

[2]Institute for Clinical Neurobiology, University of Wuerzburg, Versbacherstr. 5, 97078 Wuerzburg, Germany

[3]The Francis Crick Institute, Midland Rd, London, NW1 1AT, UK

[4]Department of Neuromuscular Disease, UCL Institute of Neurology, Queen Square, London, WC1N 3BG, UK

[5]Division of Brain Sciences, Department of Medicine, Imperial College London, London, WC12 0NN, UK

[6]Institute of Molecular Biology (IMB) GmbH, Ackermannweg 4, 55128 Mainz, Germany

[7]The Medical Research Council Cancer Unit, University of Cambridge, Hills Road, Cambridge, CB2 0XZ, UK

[8]RNA Biology and Cancer Laboratory, Peter MacCallum Cancer Centre, 305 Grattan Street, Melbourne, Australia, 3000

[9]Department of Genetics, Environment and Evolution, UCL Genetics Institute, Gower Street, London WC1E 6BT, UK

[10]Okinawa Institute of Science & Technology Graduate University, 1919-1 Tancha, Onna-son, Kunigami-gun, Okinawa 904-0495, Japan

[11]Department of Biochemistry, University of Cambridge, Downing Site, Tennis Court Road, Cambridge, CB2 1QW, UK

[12]Faculty of Computer and Information Science, University of Ljubljana, Ljubljana, Slovenia

Author Information:
Michael Briese, Nejc Haberman and Christopher R Sibley contributed equally to this work.

Corresponding author:
[§]Jernej Ule: jernej.ule@crick.ac.uk

Abstract

Studies of spliceosomal interactions are challenging due to their dynamic nature. Here we employed spliceosome iCLIP, which immunoprecipitates SmB along with snRNPs and auxiliary RNA binding proteins (RBPs), to map human spliceosome engagement with snRNAs and pre-mRNAs. This identified over 50,000 branchpoints (BPs) that have canonical sequence and structural features. Moreover, it revealed 7 binding peaks around BPs and splice sites, each precisely overlapping with binding profiles of specific splicing factors. We show how the binding patterns of these RBPs are affected by the position and strength of BPs. For example, strong or proximally located BPs preferentially bind SF3 rather than U2AF complex. Notably, these effects are partly neutralized during spliceosomal assembly in a way that depends on the core spliceosomal protein PRPF8. These insights exemplify spliceosome iCLIP as a broadly applicable method for transcriptomic studies of splicing mechanisms.

Introduction

Splicing is a multi-step process in which multiple small nuclear ribonucleoprotein particles (snRNPs) and associated splicing factors bind at specific positions around intron boundaries in order to assemble an active spliceosome through a series of remodeling steps. The splicing reactions are coordinated by dynamic pairings between different snRNAs, between snRNAs and pre-mRNA, and by protein-RNA contacts[1]. Transcriptome-wide studies of splicing reactions can be particularly valuable to unravel the multi-component and dynamic assembly of the spliceosome on the pre-mRNA substrate[2-4]. In yeast, "spliceosome profiling" has been developed through affinity purification of the tagged U2·U5·U6·NTC complex from *Schizosaccharomyces pombe* to monitor its interactions using a RNA footprinting-based strategy[2,3]. It is currently unclear if this method can be applied to mammalian cells, which might be more sensitive to the introduction of affinity tags into splicing factors. Moreover, a method is needed to simultaneously monitor the full complexity of the interactions of diverse RBPs on pre-mRNAs from the earliest to the latest stages of spliceosomal assembly.

A second challenge in understanding splicing mechanisms is the need to assign the position of branchpoints (BPs). The sequence consensus of mammalian BPs is less well defined compared to yeast, therefore experimental methods are important to validate computational predictions. High-throughput methods to identify BPs have so far relied on lariat-spanning RNA-seq reads that cross from the 5' portion of the intron, over the BP, and finally finish in the 3' portion of the intron upstream of the BP[5-7]. However, lariat-spanning RNA-seq reads are very rare, and therefore experimental annotation of BPs remains incomplete. In yeast, spliceosome profiling was successful in assigning the positions of BPs by monitoring the position of cDNAs truncating at BPs[2], indicating that a similar approach could also be applied to mammalian cells.

Here, we have adapted the individual nucleotide resolution UV crosslinking and immunoprecipitation (iCLIP) method[8] to develop spliceosome iCLIP. This represents a new approach that defines positions of spliceosomal crosslinks on pre-mRNAs at nucleotide resolution[4] and, thereby, simultaneously maps the crosslink profiles of core and accessory spliceosomal factors that are known to participate across the diverse stages of the splicing cycle. Due to the nucleotide precision of iCLIP, we could distinguish 7 binding peaks, corresponding to distinct RBPs that differ in their requirement for ATP or for the factor PRPF8. Spliceosome iCLIP also purifies intron lariats, which identified BPs in ~64% of introns within expressed human genes. Compared to the BPs identified by RNA-seq, those identified by spliceosome iCLIP contain more canonical sequence and structural features. We have further examined the binding profiles of spliceosomal RBPs around the BPs. This demonstrates that the assembly of SF3 and associated spliceosomal complexes tends to be determined by a primary BP in most introns, even though alternative BPs are detected by lariat-derived reads. Moreover, we identify complementary roles of U2AF and SF3 complexes in BP definition. Taken together, these findings demonstrate the value of spliceosome iCLIP for transcriptomic studies of BP definition and spliceosomal interactions with pre-mRNAs.

Results

Spliceosome iCLIP identifies interactions between splicing factors, snRNAs and pre-mRNAs

SmB/B' proteins are part of the highly stable Sm core common to all spliceosomal snRNPs except U6[1], making them suitable candidates for enriching snRNPs via immunopurification. In order to adapt iCLIP for the study of a multi-component machine like the spliceosome, we used antibodies against the endogenous SmB/B' proteins[9] using a range of conditions with differing stringency of detergents and salt concentration for the lysis and washing steps (Supplementary Table 1, Fig. 1a and Supplementary Fig. 1a,b). To enable denaturing purification, we generated HEK293 cells stably expressing Flag-tagged SmB and employed urea to purify SmB via a Flag tag, which minimizes co-purification of additional proteins[10] ('stringent' purification, Supplementary Table 1). We observed a 25 kDa band corresponding to the molecular weight of SmB-RNA complex, which was absent in controls (Supplementary Fig. 1c). Next, we employed the standard, non-denaturing iCLIP condition ('medium' stringency), which employs a high concentration of detergents in the lysis buffer, and a washing buffer with 1M NaCl ('medium' purification, Supplementary Table 1). This disrupts most protein-protein interactions, but can preserve stable complexes such as snRNPs, which is evident by the multiple radioactive bands in addition to the 25 kDa SmB-RNA complex upon treatment with low RNase (Fig. 1b). No radioactive signal was detected if the SmB/B' antibody was omitted during immunopurification (Fig. 1b and Supplementary Fig. 1d). To co-purify additional accessory splicing factors, we further decreased the concentration of detergents in the lysis buffer, and used only 0.1M NaCl in the washing buffer ('mild' purification, Supplementary Table 1). Under this condition, the diffuse signal at 30-200 kDa strongly increased compared to the medium condition, indicating that the mild condition allows the most efficient purification of proteins associated with snRNPs (Fig. 1a and Supplementary Fig. 1e). Under the low RNase treatment, snRNAs remain more intact, and they can thereby serve as a scaffold for purifying the multi-protein spliceosomal complex (Fig. 1a). A similar radioactive labeling pattern was obtained when using three different monoclonal SmB/B' antibodies (Supplementary Fig. 1d).

To produce cDNA libraries with spliceosome iCLIP, we immunoprecipitated SmB under the three different stringency conditions from lysates of UV-crosslinked cells or tissue, and isolated a broad size distribution of protein-RNA complexes in order to recover the greatest possible diversity of spliceosomal protein-RNA interactions (Fig. 1b and Supplementary Fig. 1c-e). Mouse brain tissue was used for medium and mild purification with an antibody against endogenous SmB/B', and HEK293 cells expressing Flag-tagged SmB for stringent, denaturing purification with anti-Flag antibody. As in previous iCLIP studies[8], the nucleotide preceding each cDNA was used for all analyses. When stringent conditions were used, >75% of iCLIP cDNAs mapped to snRNAs, likely corresponding to the direct binding of Flag-tagged SmB (Fig. 1c). However, the proportion of snRNA crosslinking was reduced to approximately 10% under mild and

135 medium conditions, with a corresponding increase of crosslinking to introns and exons,
136 which likely reflects binding of snRNP-associated proteins to pre-mRNAs (Fig. 1a,c).

137 **Spliceosome iCLIP identifies seven crosslinking peaks on pre-mRNAs**

138 Assembly of the spliceosome on pre-mRNA is guided by three main landmarks: the 5'ss,
139 3'ss and BP. Therefore, we evaluated if spliceosomal crosslinks are located at specific
140 positions relative to boundaries of annotated exons and to computationally predicted
141 BPs[11]. For this purpose, we performed spliceosome iCLIP from human Cal51 cells, which
142 have been use as a model system to study the roles of spliceosomal factors in cell cycle[4].
143 RNA maps of summarized spliceosomal crosslinking revealed 7 peaks of crosslinking
144 around these landmarks, with same positional pattern in Cal51 cells and mouse brain
145 (Fig. 2a and Supplementary Fig. 2a). The centers of the peaks were seen at 15 nt
146 upstream of the 5'ss (peak 1), 10 nt downstream of the 5'ss (peak 2), 31 nt downstream
147 of the 5'ss (peak 3), 26 nt upstream of the BP (peak 4), 20 nt upstream of the BP (peak
148 5), 11 nt upstream of the 3'ss (peak 6) and 3 nt upstream of the 3'ss (peak 7). We also
149 observed alignment of cDNA starts to the start of the intron and the BPs, which we refer
150 to as positions A and B which are discussed below in more detail (Fig. 2a and
151 Supplementary Fig. 2a).

152 The enrichment of crosslinking at most peaks was generally stronger under the mild
153 condition, especially at the 3'ss, in agreement with the stronger signal of co-purified
154 complexes on the SDS-PAGE gel (Supplementary Fig. 1e and 2a). This indicates that
155 spliceosome iCLIP performed under mild conditions is most suitable for investigating
156 spliceosomal assembly on pre-mRNAs. We therefore used the mild condition to
157 investigate how PRPF8 knockdown (KD) affects spliceosomal interactions in Cal51 cells
158 (Supplementary Fig. 2b). PRPF8 is an integral U5 snRNP component, and therefore part
159 of complexes B and C, where it contacts residues of U5 and U6 snRNAs, as well as pre-
160 mRNA at both the splice sites and BP[1]. We have previously used spliceosome iCLIP to
161 show that PRPF8 is essential for efficient spliceosomal assembly at 5'ss[4]. Here we
162 additionally find that PRPF8 is essential for efficient spliceosomal assembly at peaks 4-5
163 (Fig. 2a). Moreover, we also observed a major decrease of reads truncating at the
164 positions A and B, whereas crosslinking at peaks 2 and 6 is increased upon PRPF8 KD.
165 Thus, the peaks of spliceosomal crosslinking vary in their sensitivities to PRPF8
166 depletion.

167 ***In vitro* spliceosome iCLIP defines the ATP-dependence of crosslinking peaks**

168 In order to verify that spliceosome iCLIP is able to represent multiple stages of the
169 splicing reaction, we performed an *in vitro* splicing assay using defined conditions. We
170 added an exogenous pre-mRNA splicing substrate to HeLa nuclear extract in the
171 presence or absence of ATP. The RNA substrate was produced by *in vitro* transcription
172 of a minigene construct containing a short intron and flanking exons from the human
173 *C6orf10* gene. Gel electrophoresis analysis of splicing products confirmed that ATP was
174 required for the formation of intron lariats and other splicing products (Supplementary
175 Fig. 2c). We performed spliceosome iCLIP from the splicing reactions using the mild

176 purification condition (Supplementary Fig. 2d). Upon sequencing, the reads mapping to
177 the exogenous splicing substrate or the spliced product represented ~1%, whereas the
178 remaining 99% of mapped reads were derived from endogenous RNAs that are present
179 in the nuclear extract. The spliced product was detected with exon-exon junction reads
180 primarily in the presence of ATP (364 reads in +ATP vs. 5 reads in -ATP condition)
181 (Supplementary Fig. 2e and Supplementary Table 4). Of note, in the +ATP condition the
182 reads mapping to the spliced product (364 reads) were much lower compared to those
183 mapping to the unspliced substrate (48,584 reads) (Supplementary Table 4), as
184 expected given that the spliceosome rapidly disassembles upon completion of the
185 splicing reaction.

186 We visualized the crosslinking on the substrate RNA, and marked the positions of peaks
187 that corresponded best to those found on endogenous transcripts (Fig. 2b). Whilst
188 crosslinking sites detected on a metagene plot might not necessarily be representative
189 of individual splicing substrates, we nevertheless observed crosslinking peaks in regions
190 of the *C6orf10* substrate at similar positions to the transcriptome-wide peaks
191 (comparing Fig. 2a and 2b). When comparing crosslinking in the presence or absence of
192 ATP, a reproducible crosslinking profile was seen at peaks 1, 2, 6 and 7, indicating that
193 these crosslinks correspond to ATP-independent contacts of early spliceosomal factors.
194 In contrast, the presence of ATP increased the signal at several other peaks: we
195 observed a ~9 fold increase at peaks 4 and 5, located upstream of the BP, which are also
196 dependent on PRPF8 *in vivo* (Fig. 2a). This indicates that spliceosome iCLIP detects pre-
197 mRNA binding of factors that contribute to distinct stages of spliceosomal assembly.

198 **Lariat-derived reads are readily obtained by spliceosome iCLIP**
199
200 Following crosslinking, the peptide that remains bound to the RNA after digestion of the
201 RBP can lead to termination of reverse transcription and produce the so-called
202 'truncated cDNAs'[12]. The predominance of truncated cDNAs in iCLIP libraries has been
203 validated by multiple means[13,14], and therefore our analysis of iCLIP data generally
204 refers to the nucleotide preceding the iCLIP read on the reference genome as the
205 'crosslink site'. The same applies to derived methods, such as eCLIP[15]. In spliceosome
206 iCLIP, we expect that cDNAs could also truncate at the three-way junction formed by
207 intron lariats, where the 5' end of the intron is linked via a 2'-5' phosphodiester bond to
208 the BP (Fig. 2c). Such three-way-junction RNAs present two available 3' ends for ligation
209 to adapters, and these reads could truncate at the BP (i.e. position B) or at the start of
210 the intron (i.e. position A), especially if the RBP crosslink site is located upstream of the
211 BP. Indeed, we find strong alignment of cDNA starts at positions A and B, which is
212 dramatically decreased under conditions that decrease the presence of intron lariats:
213 PRPF8 KD *in vivo* (2-fold, Fig. 2a), or the absence of ATP *in vitro* (>15-fold, Fig. 2b).
214 Interestingly, the medium purification condition was optimal to produce cDNAs that
215 truncate at the positions A and B (Supplementary Fig. 2a), possibly because
216 spliceosomal C complexes are readily obtained under high-salt conditions[16].
217
218 **Spliceosome iCLIP identifies >50,000 human branchpoints (BPs)**

219 We performed twelve spliceosome iCLIP experiments under medium purification
220 conditions from UV-crosslinked Cal51 cells that were synchronized at 4 stages of cell
221 cycle, with three replicates for each stage (see Methods). We first confirmed that the
222 starts of spliceosome iCLIP cDNAs generally overlap with a uridine-rich motif (Fig. 3a),
223 in agreement with the increased propensity of protein-RNA crosslinking at uridine-rich
224 sites[13]. In contrast, the nucleotide composition at the starts of cDNAs that end at the last
225 nucleotide of introns strongly overlaps with the YUNAY motif, the consensus sequence
226 of BPs (Fig. 3b). Further, these cDNAs have higher enrichment of mismatches of
227 adenosines at their first nucleotide (Supplementary Fig. 3a), which is consistent with
228 mismatch, insertion and deletion errors during reverse transcription across the three-
229 way junction of the BP[7]. Thus, cDNAs overlapping with intron ends appear to be derived
230 from intron lariats, such that they truncate at the three-way junctions at BPs rather than
231 at crosslink sites of RBPs. In total, they identify 132,287 sites in introns, which could be
232 considered as candidates for BP positions (Fig. 3b).

233 To identify a confident set of putative BPs in a transcriptome-wide manner, we used the
234 spliceosome iCLIP cDNAs that overlap with intron ends in 9,363 genes with FPKM>10
235 (as determined by RNA-seq) in Cal51 cells. Thereby we wished to ensure that the genes
236 were expressed at a level that was sufficient for confident analysis of introns. Initially,
237 we only used those cDNAs that overlapped with the end of introns, since we found that
238 these cDNAs tend to start at a BP consensus motif (Fig. 3b). These cDNAs started at
239 adenines in 35,056 introns, which we considered as putative BPs. The more distal BPs
240 would not be identified by this approach due to our 41 read-length limit, and therefore
241 we proceeded to a second step in introns where the initial approach did not identify any
242 BPs. We analyzed all cDNAs, and overlapped their truncation sites with BPs
243 computationally predicted in 2010[17], in order to maintain independence from the more
244 recently computationally predicted BPs that are used for later comparisons in our
245 paper[11]. We selected the positions of computationally predicted BPs with the highest
246 number of truncated cDNAs, which identified candidate BPs in another 15,756 introns.
247 Collectively, this identified candidate BPs in 50,812 introns of 9,363 genes. These genes
248 in total contain 78,894 annotated introns, and thus iCLIP identified putative BPs in 64%
249 of introns in expressed genes.

250 **BPs identified by iCLIP contain canonical sequence and structural features**

251 To examine the 50,812 BPs identified by spliceosome iCLIP ('iCLIP BPs'), we compared
252 them with the 'computational BPs' identified recently with a sequence-based deep
253 learning predictor, LaBranchoR, which predicted a BP for over 90% of 3'ss[11]. We also
254 compared with the 'RNA-seq BPs', including the 130,294 BPs from 50,810 introns that
255 were identified by analysis of lariat-spanning reads from 17,164 RNA-seq datasets[6].
256 61% of iCLIP BPs overlapped with the top-scoring computational BPs (Supplementary
257 Fig. 3b). Interestingly, in cases where iCLIP and computational BPs are located <5 nt
258 apart, they tend to occur within A-rich sequences (Supplementary Fig. 3c). This
259 mismatch could be of technical nature, as truncation of iCLIP cDNAs may not be always
260 precisely aligned to the BPs in case of A-rich sequences, or alternatively multiple As
261 might be capable of serving as BPs when they are located in close vicinity. We therefore

262 allowed 1 nt shift for comparison between methods, as has been done previously[11],
263 which showed that 68% of iCLIP BPs overlapped with the top-scoring computational
264 BPs, and 26% overlapped with the RNA-seq BPs (Fig. 3c). If the computational BPs
265 overlapped either with an iCLIP BP and/or RNA-seq BP, it generally had a strong BP
266 consensus motif (o-BP, Fig. 3d).

267 To gain insight into the features of BPs that are unique to each method, we then focused
268 on BPs that were identified by a single method and were >5 nt away from BPs identified
269 by other methods. Notably, the computational- or iCLIP-specific BPs have a strong
270 enrichment of the consensus YUNAY motif (c-BP, i-BP, Fig. 3e,f,h,i). In contrast, the RNA-
271 seq-specific BPs contain a larger proportion of non-canonical BP motifs, which agrees
272 with previous observations[5,7,11] (Fig. 3g,j). To evaluate this further, we compared the
273 iCLIP BPs with two studies that identified 59,359 BPs by exoribonuclease digestion and
274 targeted RNA-sequencing[7], and 36,078 BPs by lariat-spanning reads refined by
275 U2snRNP/pre-mRNA base-pairing models[5]. Considering the introns that contained BPs
276 defined both by RNA-seq and iCLIP, we found 55% and 45% overlapping BPs to each
277 study (Supplementary Fig. 3d-g). Again, the iCLIP-specific BPs were more strongly
278 enriched in the consensus YUNAY motif compared the BPs that are specifically identified
279 by either RNA-seq method (Supplementary Fig. 3h-m).

280 Finally, we examined the local RNA structure around each category of BPs. Overlapping,
281 iCLIP-specific and computational-specific BPs had a strong propensity for single-
282 stranded RNA at the position of the BP, which was not seen for the RNA-seq-specific BPs
283 (Fig. 3k,l). This indicates that the RNA-seq-specific BPs might be structurally less
284 accessible for pairing with U2 snRNP. In conclusion, we find that BPs identified by
285 spliceosome iCLIP contain the expected sequence and structural features.

286 **Specific RBPs are enriched at each peak of spliceosomal crosslinking**

287 Next, we assessed which RBPs might correspond to the peaks identified by spliceosome
288 iCLIP to play a role in BP recognition (peaks 4-7) or formation of intron lariats
289 (positions A and B). We examined published iCLIP data produced in our lab for 18
290 previously studied RBPs[18-22], and eCLIP data from K562 and HepG2 cells for 110 RBPs
291 provided by the ENCODE consortium[15] to assess normalized crosslinking at each peak.
292 This identified a set of RBPs enriched at each peak (Fig. 4 and Supplementary Table 5).
293 As expected, SF3 components SF3B4, SF3A3 and SF3B1 bind to peaks 4-5[23], U2AF2
294 binds the polypyrimidine (polyY) tract (peak 6), and U2AF1 close to the intron-exon
295 junction (peak 7)[21].

296 **RBP binding profiles signify the functionality of BPs**

297 Peaks 4-6 and position B align to BP position, and therefore we could evaluate how the
298 crosslinking profiles of RBPs that bind at these peaks align to the different classes of
299 BPs. First, we examined the crosslinking of SF3B4, which binds in the region of peak 4
300 as part of the U2 snRNP complex that recognises the BP[1]. Analysis of the overlapping

301 BPs (o-BP) defines the peak of SF3B4 crosslinking at the 25th nt upstream of BPs (Fig. 5
302 and Supplementary Fig. 4a,b). However, the peak of SF3B4 crosslinking doesn't overlap
303 as well to this 25th position for the non-overlapping, method-specific BPs; it is generally
304 closer than 25 nt to the BPs that are located upstream of another BP (up BP), and further
305 than 25 nt awat from BPs that are located downstream of another BP (down BP) (Fig. 5).
306 The shift from the expected position is greatest for the RNA-seq-specific BPs (R-BP), and
307 smallest for the computationally predicted BPs, as evident by eCLIP data from two cell
308 lines (Fig. 5a,b). Moreover, the same result is seen with U2AF2, where the strongest shift
309 away from expected positions is seen for RNA-seq BPs, and weakest for computational
310 BPs (Supplementary Fig. 4c,d). Given that computationally predicted BPs align best to
311 the SF3 and U2AF binding profiles, we conclude that spliceosome assembles most
312 efficiently on these BPs.

313 The cDNA starts from PRPF8 eCLIP are highly enriched at position B, corresponding the
314 lariat-derived cDNAs that truncate at BPs (Fig. 4). Interestingly, the PRPF8 cDNA starts
315 had the strongest peak at the overlapping BPs, but also peaked at all the remaining
316 classes of BPs (Supplementary Fig. 4e,f). This indicates that all classes of BPs contribute
317 to lariat formation, and thus the non-overlapping BPs most likely act as alternative BPs
318 within the introns.

319 **Effects of branchpoint position on spliceosomal assembly**

320 To assess how the position of BPs determines spliceosome assembly, we evaluated the
321 binding profiles of the RBPs that are enriched at peaks 4-7 and at positions A and B (Fig.
322 4). We divided BPs based on their distance from 3'ss, and normalized the RBP binding
323 profiles within each subclass of BPs. This showed that crosslinking of U2AF1 and U2AF2
324 aligns to the region between the BPs and 3'ss, which is covered by the polyY tract
325 (Supplementary Fig. 5 and 6). SF3B4 is the primary RBP crosslinking at peak 4, and
326 SF3A3 at 5, and SMNDC1, SF3B1, EFTUD2, BUD13, GPKOW and XRN2 bind to peaks 4/5
327 (Supplementary Fig. 5, 6 and Fig. 4). PRPF8, RBM22 and SUPV3L1 have their cDNA
328 starts truncating at positions A and B (Supplementary Fig. 5 and 6), corresponding to
329 the three-way junction formed by intron lariats (Fig. 2c), in agreement with the
330 association of PRPF8 and RBM22 with intron lariats as part of the human catalytic step I
331 spliceosome[1].

332 In order to quantify how the position of BPs affects the intensity of RBP binding, we
333 divided BPs into 10 equally sized groups based on the distance from 3'ss. We then
334 normalized the relative binding intensity of each RBP at each position on the RNA maps
335 across the ten groups, which revealed strong relationships between BP position and
336 binding intensity of certain RBPs (Fig. 6a, Supplementary Fig. 7a). For example, if a BP is
337 located distally from the 3'ss, then U2AF components bind stronger to peaks 6/7. In
338 contrast, if a BP is located proximally to the 3'ss, then EFTUD2, SF3 components and
339 several other RBPs bind stronger to the peaks 4 or 5 (Fig. 6b). Notably, increased BP
340 distance causes increased binding of BUD13 and GPKOW at peaks 6/7 and decreased
341 binding at peaks 4/5. The more efficient recruitment of U2AF and associated factors to
342 peaks 6/7 could be explained by the long polyY-tracts at distal BPs (Supplementary Fig.

343 5), while their decreased binding at proximal BPs appears to be compensated for by the
344 increased binding of SF3 and other U2 snRNP-associated factors at peaks 4/5.

345 In contrast to the effects on individual splicing factors, the relative intensity of
346 spliceosome iCLIP crosslinking in peaks 4/5 compared to 6/7 was not visibly changed in
347 relation to BP distance (Fig. 6c). This indicates that the differences in the binding
348 patterns of individual splicing factors might be neutralized during spliceosomal
349 assembly. To ask if this is the case, we turned to PRPF8, a protein that is essential for the
350 last stage of spliceosome assembly, a role it plays together with EFTUD2 and BRR2 as
351 part of U5 snRNP[1]. PRPF8 knockdown leads to decreased spliceosomal binding at peaks
352 4/5, and this effect is stronger at distal compared to proximal BPs (Fig. 6c). In
353 conclusion, our results reveal differences in the binding profiles of splicing factors in
354 relation to BP distance, but these differences are neutralized upon spliceosome
355 assembly in a manner that requires the presence of PRPF8.

356 **Effects of branchpoint strength on spliceosomal assembly**

357 We also wished to examine how the strength of consensus BP sequence affects
358 spliceosomal assembly. For this purpose, we focused on BPs that are located at 23-28 nt
359 upstream of the 3'ss, which is the most common positions of BPs (20,018 BPs,
360 Supplementary Table 6). As an estimate of BP strength we used the BP score, which was
361 determined with a deep-learning model[11]. This showed strong correlation between BP
362 strength and binding intensity of certain RBPs (Fig. 7a, Supplementary Fig. 7b). Among
363 others, increased binding of U2AF is seen at peak 7 of weak BPs, and increased binding
364 of SF3B4 at peaks 4/5 of strong BPs (Fig. 7b). Notably, an over 4-fold change is seen in
365 the ratio between the U2AF and SF3 complexes when comparing the extreme deciles of
366 BP strength ($p<0.001$, Wilcoxon Rank Sum test, Supplementary Fig. 7c). We did not
367 observe any correlation between the polyY tract coverage and BP score, which indicate
368 that the change in binding profiles is a direct result of BP consensus variation
369 (Supplementary Fig. 7d). Notably, in case of several RBPs, such as XRN2 and SF3B1,
370 weak BP scores correlated with a strong decrease in binding at peaks 6/7 as well as an
371 increase in binding at peaks 4/5 (Fig. 7b).

372 Similar to the effects on individual splicing factors, the relative intensity of spliceosome
373 iCLIP crosslinking in peaks 4/5 was increased with increasing BP strength (Fig. 7c,
374 compare the blue lines on the left and right graphs). PRPF8 knockdown decreased
375 spliceosomal binding at peaks 4/5 of both classes of BPs, and this led to stronger
376 crosslinking at peaks 6/7 relative to peaks 4/5 at weak BPs, even though the peaks 4/5
377 are usually stronger. The signal at position B of weak BPs is almost completely lost upon
378 PRPF8 knockdown, which likely reflects the absence of intron lariats due to perturbed
379 splicing of introns with weak BPs (Fig. 7c). In conclusion, our results suggest that BP
380 strength affects the assembly efficiency of spliceosomal factors at peaks 4/5, which
381 could contribute to the variations between introns in their sensitivity to perturbed
382 spliceosome function.

383

384 **Discussion**

385 Here we established spliceosome iCLIP to study the interactions of endogenous snRNPs
386 and accessory splicing factors on pre-mRNAs. We identified primary peaks of
387 spliceosomal protein-pre-mRNA interactions, which precisely overlap with crosslinking
388 profiles of 15 splicing factors. Moreover, the presence of lariat-derived reads in
389 spliceosome iCLIP identified >50,000 BPs, which have canonical sequence and structural
390 features. Due to the precise alignment of splicing factors to the positions of BPs, we
391 could use their binding profiles to show that the assembly of U2 snRNP is primarily
392 coordinated by the computationally predicted BPs, whilst the alternative BPs that are
393 identified only by iCLIP or RNA-seq are more rarely used. Finally, we reveal the major
394 effect of the position and strength of BPs on spliceosomal assembly, which can explain
395 why distally located as well as weak BPs are particularly sensitive to perturbed
396 spliceosome function upon PRPF8 KD. These findings demonstrate the broad utility of
397 spliceosome iCLIP for simultaneous and transcriptome-wide analysis of the assembly of
398 diverse spliceosomal components.

399 **The value of spliceosome iCLIP for identifying BPs**

400 Experimental methods to identify BPs, which rely on reads from RNA-seq or iCLIP, are
401 based on cDNAs derived from intron lariats. A caveat of these methods is that the
402 stability of intron lariats depends on the kinetics of debranching and intron degradation,
403 which may be affected by the properties of BPs. One study indicates that lariats formed
404 at non-canonical BPs are less efficiently debranched[24], which would increase the
405 detection of non-canonical BPs by experimental methods. iCLIP captures a snapshot of
406 RBP-RNA interactions that are in complex with spliceosome, which should minimize any
407 biases of lariat stability. This could explain why the BPs identified by iCLIP contain a
408 stronger consensus sequence and higher structural accessibility than the BPs that had
409 been identified with lariat-spanning reads in RNA-seq. The reason for this difference
410 may lie in the fact that lariats identified by iCLIP are in complex with the spliceosome at
411 the time of crosslinking. The methods that rely on RNA-seq are expected to be more
412 sensitive to the variable stability of intron lariats after their release from the
413 spliceosome, which could lead to their greater propensity for detecting non-canonical
414 BPs. The further value of spliceosome iCLIP is that, in addition to experiments under the
415 medium condition, which serves for BP identification through lariat-derived cDNAs,
416 experiments under the mild condition identify crosslinking of the RBPs in peaks 4/5 that
417 align to BPs, thus enabling validation of BPs that is independent of variable lariat
418 abundance (Fig. 5). Thus, a combined use of spliceosome iCLIP at both conditions is
419 valuable to study the functionally relevant BPs, especially when combined with
420 computational modelling of BPs[11].

421 **The role of BP position and strength in spliceosomal assembly**

422 We show that BP position and the computationally defined strength of BPs correlate
423 with the relative binding of dozens of splicing factors around BPs. This is exemplified by
424 strong binding of SF3 components at strong BPs, or BPs located close to 3'ss, whilst

425 U2AF components bind stronger to weak BPs, or BPs located further from 3'ss. In cases
426 of SF3B1, BUD13 and GPKOW, we observed enriched binding both at peaks 4/5 as well
427 as 6/7, with reciprocal changes between the two peaks that depend on the features of
428 BPs (Fig. 6 and 7). These RBPs are not known to bind at peaks 6/7, and it is plausible
429 that signal at some peaks represents binding of U2AF or other spliceosomal factors that
430 are co-purified during eCLIP. It is presently not possible to fully distinguish between
431 direct and indirect binding, because the purified protein-RNA complexes have not been
432 visualized after their separation on SDS-PAGE gels in eCLIP[12]. Nevertheless, our data
433 clearly show that BP characteristics determine the balance of interactions between
434 peaks 4/5 and 6/7 for a broad range of spliceosomal factors.

435 Our findings show a good convergence of transcriptomic insights with CryoEM studies
436 of spliceosome structure. The RBPs with strongest enrichment at peaks 4/5 include
437 SF3B4, SF3B1 and SF3A3, which are required for the ATP-dependent step of
438 spliceosome assembly on the BPs[25]. This is in agreement with the ATP-dependence of
439 peaks 4 and 5 *in vitro* and their disruption by PRPF8 KD. The binding positions of SF3B4
440 (peak at 26 nt upstream of BPs) and SF3A3 (peak at 15 nt upstream of BPs) is consistent
441 with the structure of the human activated spliceosome, where SF3A3 (also referred to as
442 SF3a60) binds to pre-mRNA at a position closer to the BP compared to SF3B4 (also
443 referred to as SF3b49)[26]. Interestingly, while we observe binding peaks in the region 19-
444 26 nt upstream of BPs in humans, the late spliceosomal components in yeast had their
445 peak centered at ~48-49 nt upstream of BPs[2]. In both cases, these contacts don't overlap
446 with any sequence motif, and thus their binding position appears to be defined by the
447 assembly of the spliceosome on BPs. The constrained conformation of the larger
448 spliceosomal complex appears to act as a molecular ruler that positions each associated
449 RBP on pre-mRNAs at a specific distance from BPs.

450 In conclusion, spliceosome iCLIP monitors concerted pre-mRNA binding of many types
451 of spliceosomal complexes with nucleotide resolution, allowing their simultaneous
452 study due to the distinct position-dependent binding pattern of components that act at
453 multiple stages of the splicing cycle. The method can be used to study endogenous
454 spliceosome and BPs at multiple stages of development, and across tissues and species,
455 without the need for protein tagging that was used in yeast[2,3]. Several spliceosomal
456 components, including U2AF1, SF3B1 and PRPF8, are targets for mutations in myeloid
457 neoplasms, retinitis pigmentosa and other diseases[27]. Spliceosome iCLIP could now be
458 used to monitor global impacts of these mutations on spliceosome assembly in human
459 cells. More generally, our study demonstrates the value of iCLIP for monitoring the
460 position-dependent assembly and dynamics of multi-protein complexes on endogenous
461 transcripts.

462

463

464 **Acknowledgements**

465 We thank Livio Pellizzoni for the 18F6 monoclonal antibody, Miriam Llorian for help
466 with the *in vitro* splicing reactions, Kathi Zarnack and Gregor Rot for help with the data
467 analyses, and Lisa Strittmatter and members of Ule lab for helpful discussions and
468 comments on the manuscript. This work was supported primarily by the European
469 Research Council (206726-CLIP and 617837-Translate) and the Slovenian Research
470 Agency (P2-0209, Z7-3665, J7-5460). CRS is supported by an Edmond Lily Safra
471 fellowship. AMC is supported by a Wellcome Trust PhD Training Fellowship for
472 Clinicians (110292/Z/15/Z). DP and VOW were supported by Medical Research Council
473 programme grants MC_UU_12022/1 and MC_UU_12022/8 to ARV. The Francis Crick
474 Institute receives its core funding from Cancer Research UK (FC001002), the UK Medical
475 Research Council (FC001002), and the Wellcome Trust (FC001002).

476 **Author contributions**

477 MB, CRS and JU conceived the project, designed the experiments and wrote the
478 manuscript, with assistance of all co-authors. MB, CRS and ZW performed experiments,
479 with assistance from JU, JK and CWS. NH performed most computational analyses, with
480 assistance from CRS, TC, AMC and NML. VOW, DP and ARV provided crosslinked pellets
481 from wild-type and PRPF8-depleted Cal51 cells.

482 **Declaration of Interests**

483 The authors declare no competing interests.

484

485

486

487

488

489 **References:**

490 1 Fica, S. M. & Nagai, K. Cryo-electron microscopy snapshots of the
491 spliceosome: structural insights into a dynamic ribonucleoprotein
492 machine. *Nat Struct Mol Biol* **24**, 791-799, doi:10.1038/nsmb.3463
493 (2017).
494 2 Chen, W. *et al.* Transcriptome-wide Interrogation of the Functional
495 Intronome by Spliceosome Profiling. *Cell* **173**, 1031-1044 e1013,
496 doi:10.1016/j.cell.2018.03.062 (2018).
497 3 Burke, J. E. *et al.* Spliceosome Profiling Visualizes Operations of a Dynamic
498 RNP at Nucleotide Resolution. *Cell* **173**, 1014-1030 e1017,
499 doi:10.1016/j.cell.2018.03.020 (2018).
500 4 Wickramasinghe, V. O. *et al.* Regulation of constitutive and alternative
501 mRNA splicing across the human transcriptome by PRPF8 is determined
502 by 5' splice site strength. *Genome Biol* **16**, 201, doi:10.1186/s13059-015-
503 0749-3 (2015).
504 5 Taggart, A. J. *et al.* Large-scale analysis of branchpoint usage across
505 species and cell lines. *Genome Res* **27**, 639-649,
506 doi:10.1101/gr.202820.115 (2017).
507 6 Pineda, J. M. B. & Bradley, R. K. Most human introns are recognized via
508 multiple and tissue-specific branchpoints. *Genes Dev* **32**, 577-591,
509 doi:10.1101/gad.312058.118 (2018).
510 7 Mercer, T. R. *et al.* Genome-wide discovery of human splicing
511 branchpoints. *Genome Res* **25**, 290-303, doi:10.1101/gr.182899.114
512 (2015).
513 8 König, J. *et al.* iCLIP reveals the function of hnRNP particles in splicing at
514 individual nucleotide resolution. *Nat Struct Mol Biol* **17**, 909-915,
515 doi:nsmb.1838 [pii]
516 10.1038/nsmb.1838 (2010).
517 9 Carissimi, C., Saieva, L., Gabanella, F. & Pellizzoni, L. Gemin8 is required
518 for the architecture and function of the survival motor neuron complex. *J*
519 *Biol Chem* **281**, 37009-37016, doi:M607505200 [pii]
520 10.1074/jbc.M607505200 (2006).
521 10 Huppertz, I. *et al.* iCLIP: protein-RNA interactions at nucleotide resolution.
522 *Methods* **65**, 274-287, doi:10.1016/j.ymeth.2013.10.011 (2014).
523 11 Paggi, J. M. & Bejerano, G. A sequence-based, deep learning model
524 accurately predicts RNA splicing branchpoints. *RNA* **24**, 1647-1658,
525 doi:10.1261/rna.066290.118 (2018).
526 12 Lee, F. C. Y. & Ule, J. Advances in CLIP Technologies for Studies of Protein-
527 RNA Interactions. *Mol Cell* **69**, 354-369, doi:10.1016/j.molcel.2018.01.005
528 (2018).
529 13 Sugimoto, Y. *et al.* Analysis of CLIP and iCLIP methods for nucleotide-
530 resolution studies of protein-RNA interactions. *Genome biology* **13**, R67,
531 doi:10.1186/gb-2012-13-8-r67 (2012).
532 14 Haberman, N. *et al.* Insights into the design and interpretation of iCLIP
533 experiments. *Genome Biol* **18**, 7, doi:10.1186/s13059-016-1130-x (2017).
534 15 Van Nostrand, E. L. *et al.* A Large-Scale Binding and Functional Map of
535 Human RNA Binding Proteins. *bioRxiv*, doi:10.1101/179648 (2017).

536 16 Bessonov, S., Anokhina, M., Will, C. L., Urlaub, H. & Luhrmann, R. Isolation
537 of an active step I spliceosome and composition of its RNP core. *Nature*
538 **452**, 846-850, doi:10.1038/nature06842 (2008).
539 17 Corvelo, A., Hallegger, M., Smith, C. W. & Eyras, E. Genome-wide
540 association between branch point properties and alternative splicing.
541 *PLoS computational biology* **6**, e1001016,
542 doi:10.1371/journal.pcbi.1001016 (2010).
543 18 Wang, Z. *et al.* iCLIP predicts the dual splicing effects of TIA-RNA
544 interactions. *PLoS Biol* **8**, e1000530, doi:10.1371/journal.pbio.1000530
545 (2010).
546 19 Tollervey, J. R. *et al.* Characterizing the RNA targets and position-
547 dependent splicing regulation by TDP-43. *Nat Neurosci* **14**, 452-458,
548 doi:nn.2778 [pii]
549 10.1038/nn.2778 (2011).
550 20 Rogelj, B. *et al.* Widespread binding of FUS along nascent RNA regulates
551 alternative splicing in the brain. *Sci Rep* **2**, 603, doi:10.1038/srep00603
552 (2012).
553 21 Zarnack, K. *et al.* Direct Competition between hnRNP C and U2AF65
554 Protects the Transcriptome from the Exonization of Alu Elements. *Cell*
555 **152**, 453-466, doi:10.1016/j.cell.2012.12.023 (2013).
556 22 Attig, J. *et al.* Heteromeric RNP Assembly at LINEs Controls Lineage-
557 Specific RNA Processing. *Cell* **174**, 1067-1081 e1017,
558 doi:10.1016/j.cell.2018.07.001 (2018).
559 23 Gozani, O., Feld, R. & Reed, R. Evidence that sequence-independent
560 binding of highly conserved U2 snRNP proteins upstream of the branch
561 site is required for assembly of spliceosomal complex A. *Genes Dev* **10**,
562 233-243 (1996).
563 24 Hartmuth, K. & Barta, A. Unusual branch point selection in processing of
564 human growth hormone pre-mRNA. *Mol Cell Biol* **8**, 2011-2020 (1988).
565 25 Wahl, M. C., Will, C. L. & Lührmann, R. The spliceosome: design principles
566 of a dynamic RNP machine. *Cell* **136**, 701-718, doi:S0092-
567 8674(09)00146-9 [pii]
568 10.1016/j.cell.2009.02.009 (2009).
569 26 Zhang, X. *et al.* Structure of the human activated spliceosome in three
570 conformational states. *Cell research* **28**, 307-322, doi:10.1038/cr.2018.14
571 (2018).
572 27 Scotti, M. M. & Swanson, M. S. RNA mis-splicing in disease. *Nat Rev Genet*
573 **17**, 19-32, doi:10.1038/nrg.2015.3 (2016).
574 28 Lorenz, R. *et al.* ViennaRNA Package 2.0. *Algorithms for molecular biology :*
575 *AMB* **6**, 26, doi:10.1186/1748-7188-6-26 (2011).
576 29 Chakrabarti, A., Haberman, N., Praznik, A., Luscombe, N. M. & Ule, J. Data
577 Science Issues in Studying Protein–RNA Interactions with CLIP
578 Technologies. *Annual Review of Biomedical Data Science* **Vol. 1**,
579 doi:https://doi.org/10.1146/annurev-biodatasci-080917-013525 (2018).
580
581

582 **Legends:**

583 **Fig. 1 | Spliceosome iCLIP identifies protein interactions with snRNAs and splicing**
584 **substrates.**

585 (a) Schematic representation of the spliceosome iCLIP method performed under
586 conditions of varying purification stringency.

587 (b) Autoradiogram of crosslinked RNPs immunopurified from HeLa cells under medium
588 conditions by a SmB/B' antibody following digestion with high (++) or low (+) amounts
589 of RNase I. The dotted line depicts the region typically excised from the nitrocellulose
590 membrane for spliceosome iCLIP. As control, the antibody (Ab) was omitted during
591 immunopurification.

592 (c) Genomic distribution of spliceosome iCLIP cDNAs. For the analysis cDNAs mapping
593 to untranslated regions (UTR), coding sequence (CDS), introns and snRNAs were
594 considered. For spliceosome iCLIP under medium and mild conditions mouse brain
595 tissue was used and spliceosome iCLIP under stringent conditions was performed on
596 HEK293 cells stably expressing Flag-tagged SmB.

597 **Fig. 2 | Analysis of spliceosomal interactions with pre-mRNAs *in vitro* and *in vivo*.**

598 (a) Metagene plots of spliceosome iCLIP from Cal51 cells. Plots are depicted as RNA
599 maps of summarized crosslinking at all exon-intron and intron-exon boundaries, and
600 around BPs to identify major binding peaks, and to monitor changes between control
601 and PRPF8 knockdown (KD) cells. Crosslinking is regionally normalized to its average
602 crosslinking across the -100..50 nt region relative to 3'ss in order to focus the
603 comparison on the relative positions of peaks.

604 (b) Spliceosome iCLIP cDNA counts on the *C6orf10 in vitro* splicing substrate. Exons are
605 marked by grey boxes, intron by a line, and the BP by a green dot. The positions of
606 crosslinking peaks are marked by numbers and letters corresponding to the peaks in
607 Figure 2a.

608 (c) Schematic description of the three-way junctions of intron lariats. The three-way
609 junction is produced after limited RNase I digestion of intron lariats. This can lead to
610 cDNAs that don't truncate at sites of protein-RNA crosslinking, but rather at the three-
611 way junction of intron lariats. These cDNAs initiate from the end of the intron and
612 truncate at the BP (position B), or initiate downstream of the 5' splice site and truncate
613 at the first nucleotide of the intron (position A).

614 **Fig. 3 | Comparison of BPs identified by spliceosome iCLIP, RNA-seq lariat reads or**
615 **computational prediction.**

616 (a) Weblogo around the nucleotide preceding all spliceosome iCLIP reads.

617 (b) Weblogo around the nucleotide preceding only those spliceosome iCLIP reads that
618 align with ends of introns.

619 (c) Introns that contain at least one BP identified either by published RNA-seq[6] or by
620 spliceosome iCLIP are used to examine the overlap between the top BPs identified by
621 RNA-seq (i.e., the BP with most lariat-spanning reads in each intron), iCLIP (BP with
622 most cDNA starts) or computational predictions (highest scoring BP)[11]. BPs that are 0 or
623 1 nt apart are considered as overlapping. At the right, the explanation is given of the BP

624 categories that are used for all subsequent analyses, along with their acronyms. If a BP
625 defined by one method is >5 nt upstream of a BP defined by another method, then 'up' is
626 added to its acronym, and if it's >5 nt downstream, 'down' is added.

627 (d) Weblogo of o-BP category of BPs.

628 (e) Weblogo of C-BPup category of BPs.

629 (f) Weblogo of i-BPup category of BPs.

630 (g) Weblogo of R-BPup category of BPs.

631 (h) Weblogo of C-BPdown category of BPs.

632 (i) Weblogo of i-BPdown category of BPs.

633 (j) Weblogo of R-BPdown category of BPs.

634 (k, l) The 100 nt RNA region centered on the BP was used to calculate pairing
635 probability with RNAfold program with the default parameters[28], and the average
636 pairing probability of each nucleotide around BPs is shown for the 40 nt region around
637 method-specific BPs located upstream (k) or downstream (l).

638

639 **Fig. 4 | Identification of RBPs overlapping with spliceosomal peaks at BPs and 3'ss.**

640 To systematically identify RBPs with crosslinking peaks that overlap with each of the
641 peaks in spliceosome iCLIP, we first regionally normalized the crosslinking of each RBP
642 to its average crosslinking over -100..50 nt region relative to 3'ss, to generate the RNA
643 maps for each RBP as shown in Supplementary Fig. 5 and 6. We then ranked the RBPs
644 according to the the average normalized crosslinking across the nucleotides within each
645 peak. We analyzed peaks 4-7 and positions A and B, as marked on the top of each plot.
646 The top-ranking RBPs in each peak are shown on the left plot, and the full distribution of
647 RBP enrichments is shown on the right plot.

648

649 **Fig. 5 | Spliceosome assembly at BPs identified by spliceosome iCLIP, RNA-seq**
650 **lariat reads or computational prediction.**

651 Violin plots depicting the positioning of SF3B4 cDNA starts relative to the indicated BP
652 categories. SF3B4 eCLIP data were from K562 (a) and HepG2 (b) cells. Box-plot
653 elements are defined by center line, median; box limits, upper and lower quartiles; and
654 whiskers, 1.5x interquartile range.

655

656 **Fig. 6 | BP position defines the binding patterns of splicing factors at 3'ss.**

657 (a) Heatmaps depicting the normalized crosslinking of RBPs in peak regions around 10
658 groups of BPs that were categorized according to the distance of the BP from 3'ss.
659 Crosslinks were derived as cDNA starts from eCLIP of HepG2 cells.

660 (b) RNA maps showing normalized crosslinking profiles of selected RBPs relative to BPs
661 and 3'ss the two deciles of BPs that are located most proximal (interrupted lines) or
662 most distal (solid lines) from 3'ss.

663 (c) RNA maps showing crosslinking profile of spliceosome iCLIP from control and PRPF8
664 KD Cal51 cells in the same format as panel b.

665

666 **Fig. 7 | RNA structure around BPs correlates with the binding of splicing factors.**

667 (a) Heatmaps depicting the normalized crosslinking of RBPs in peak regions around 10
668 groups of BPs that were categorized according to the computational scores that define
669 BP strength. Crosslinks were derived as cDNA starts from eCLIP of HepG2 cells.

670 (b) RNA maps showing normalized crosslinking profiles of selected RBPs relative to BPs
671 and 3'ss the two deciles of BPs that are lowest scoring (interrupted lines) or highest
672 scoring (solid lines).

673 (c) RNA maps showing crosslinking profile of spliceosome iCLIP from control and
674 PRPF8 KD Cal51 cells in the same format as panel b.

675 (d) Schematic representation of the effects that BP position and score have on the
676 assembly of SF3 and U2AF complexes around BPs.

677

678 **Supplementary legends**

679 **Supplementary Fig. 1 | Quality control of spliceosome iCLIP with the anti-SmB/B'**
680 **antibodies**

681 (a) Western blot analysis of total HeLa cell extract with 18F6 antibody reveals a single
682 band of 28 kDa.

683 (b) Analysis of HeLa cells by immunostaining with 18F6 and epifluorescence microscopy
684 shows expected localization of SmB/B' (a speckled nuclear pattern excluding nucleoli).

685 (c) UV-crosslinked HEK FLP-in cells with stably integrated SmB-3×Flag were lysed
686 under stringent conditions and subjected to partial RNase I digestion (+, final dilution
687 1:100,000; ++, final dilution 1:5,000). Spliceosomal RNPs were immunopurified with
688 anti-Flag M2 antibody, RNA was 5' end radiolabeled, and RNPs were subjected to
689 denaturing gel electrophoresis and nitrocellulose transfer, an autoradiogram of which is
690 shown. The interrupted line indicates the area on the nitrocellulose membrane cut out
691 for purification of crosslinked RNP complexes.

692 (d) Autoradiogram of crosslinked RNPs after immunopurification with the anti-SmB/B'
693 antibodies 18F6, 12F5 or Y12 (ab3138, Abcam). HeLa cell pellet was lysed in medium
694 lysis buffer and subjected to high (++, final dilution 1:10,000) or low (+, final dilution
695 1:100,000) concentrations of RNase I. Lysates were split evenly between beads for
696 immunopurification. RNAs of immunopurified RNP complexes were radiolabeled at the
697 5' end followed by size-separation on denaturing gels and nitrocellulose transfer. The
698 time below each panel indicates length of exposure during autoradiography.

699 (e) UV-crosslinked mouse postnatal day 7 brains were lysed under medium or mild
700 stringency conditions and subjected to partial RNase I digestion (final dilution
701 1:100,000). Spliceosomal RNPs were immunopurified with anti-SmB/B' 18F6 antibody,
702 RNA was 5' end radiolabeled, and RNPs were subjected to denaturing gel
703 electrophoresis and nitrocellulose transfer, an autoradiogram of which is shown in the

704 upper panel. The interrupted line indicates the area on the nitrocellulose membrane cut
705 out for purification of crosslinked RNP complexes. For Western blotting, the remainder
706 of the supernatant following cell lysis and centrifugation was mixed with 4× NuPAGE
707 LDS sample buffer (ThermoFisher) and equal sample volumes were separated by SDS-
708 PAGE and transferred onto nitrocellulose membrane, which was incubated with anti-α-
709 tubulin antibody (1:4,000, clone B-5-1-2, cat. no. T5168, Sigma-Aldrich).

710

711 **Supplementary Fig. 2 | Analysis spliceosome iCLIP from cell extracts and *in vitro***
712 **splicing reactions.**

713 (a) RNA map of summarized crosslinking for spliceosome iCLIP performed under
714 medium or mild conditions from mouse brain around the exon-intron, intron-exon
715 junction and computationally top-scoring BP in each mouse intron[17].

716 (b) Immunoblot (IB) analysis of PRPF8 knockdown (KD) efficiency in Cal51 cells.

717 (c) RNAs transcribed *in vitro* from a *C6orf10* minigene construct were incubated with
718 HeLa nuclear extracts (NE) as part of *in vitro* splicing reactions in the presence or
719 absence of ATP. Resulting splicing products and intermediates were resolved by
720 denaturing gel electrophoresis and visualized by autoradiography.

721 (d) *In vitro* splicing reactions were diluted in mild lysis buffer, subjected to low RNase I
722 treatment (final dilution 1:200,000) and used for spliceosome iCLIP. Autoradiogram of
723 crosslinked size-separated RNP complexes show the radiolabeled RNA that is
724 crosslinked to RBPs. The interrupted line indicates the area cut out from the
725 nitrocellulose membrane for extraction of crosslinked RNAs, which were used as a
726 template for generating iCLIP cDNA libraries.

727 (e) Normalized spliceosome iCLIP cDNA counts on the *C6orf10 in vitro* splicing product.
728 Exons are marked by grey boxes. As expected, junction reads are almost exclusively
729 present only in the +ATP library.

730

731 **Supplementary Fig. 3 | Comparison of BPs determined by spliceosome iCLIP to**
732 **other methods.**

733 (a) Enrichment of mismatches at the first nucleotide of spliceosome iCLIP reads that
734 overlap with ends of introns, compared to remaining iCLIP reads.

735 (b) A table providing the number of BPs identified by spliceosome iCLIP (iCLIP BPs) in
736 introns that also contain a computationally identified BP[11]. They are divided into three
737 categories based on the distance between the iCLIP BP and the top-scoring
738 computational BP in each intron.

739 (c) Weblogo of four categories of non-overlapping BP that are $\leq$5 nt away from each
740 other, centered either on iCLIP or computational BPs, and separated according to the
741 relative position of iCLIP vs computational BP (upstream or downstream).

742 (d) The distribution of top BPs identified by published RNA-seq[7] (i.e., the BP with most
743 lariat-spanning reads in each intron) around the BPs identified by spliceosome iCLIP
744 (i.e., iCLIP BPs).

745 (e) The distribution of top BPs identified by published RNA-seq[5] (i.e., the BP with most
746 lariat-spanning reads in each intron) around the BPs identified by spliceosome iCLIP
747 (i.e., iCLIP BPs).

748 (f) A table providing the number of BPs identified by spliceosome iCLIP (iCLIP BPs) in
749 introns that also contain a BP assigned by lariat-spanning reads from RNA-seq[7]. They
750 are divided into three categories based on the distance between the iCLIP BP and the top
751 RNA-seq BP.

752 (g) A table providing the number of BPs identified by spliceosome iCLIP (iCLIP BPs) in
753 introns that also contain a BP assigned by lariat-spanning reads from RNA-seq[5]. They
754 are divided into three categories based on the distance between the iCLIP BP and the top
755 RNA-seq BP.

756 (h) Weblogo of iCLIP BPs that overlap with RNA-seq BPs[7].

757 (i) Weblogo of iCLIP BPs that are >5 nt away from RNA-seq BP[7].

758 (j) Weblogo of RNA-seq BPs[7] that are >5 nt away from iCLIP BP.

759 (k) Weblogo of iCLIP BPs that overlap with RNA-seq BPs[5].

760 (l) Weblogo of iCLIP BPs that are >5 nt away from RNA-seq BP[5].

761 (m) Weblogo of RNA-seq BPs that are >5 nt away from iCLIP BP[5].

762

763 **Supplementary Fig. 4 | Spliceosome assembly at method-specific or overlapping**
764 **BPs.**

765 RNA maps showing crosslinking (as cDNA starts from eCLIP experiments) of SF3B4
766 from K562 cells (a, b), of U2AF2 from K562 cells (c, d) and of PRPF8 from HepG2 cells (e,
767 f) relative to BPs. BPs were categorized according to the method they were specifically
768 detected by (spliceosome iCLIP, RNA-seq, computational prediction or overlapping) and
769 in case of non-overlapping BPs, according to their location relative to each other:
770 upstream (a, c, e) or downstream (b, d, f) of the other non-overlapping BP. Crosslinking
771 of each RBP is regionally normalized to its average crosslinking over -100..50 nt region
772 relative to 3'ss in order to most clearly allow comparisons between the relative
773 positions of peaks for different RBPs.

774

775 **Supplementary Fig. 5 | Crosslinking of many RBPs overlaps with peaks of**
776 **spliceosomal crosslinking.**

777 (a) Crosslinking patterns of selected RBPs, as defined by cDNA starts of eCLIP or iCLIP in
778 the indicated cell lines. Crosslinking of each is regionally normalized to its average
779 crosslinking over -100..50 nt region relative to 3'ss in order to most clearly allow
780 comparisons between the relative positions of peaks for different RBPs. All 3'ss that
781 contain BPs within 17..23 nt upstream of the exon are chosen, and crosslinking is plotted
782 in the region -40..10 nt relative to 3'ss, and -40..10 nt relative to BPs.

783 (b) Same as (a), but for all 3'ss that contain BPs within 24..39 nt upstream of the exon.

784 (c) Same as (a), but for all 3'ss that contain BPs within 40..65 nt upstream of the exon.

785

786 **Supplementary Fig. 6 | Crosslinking of many RBPs overlaps with peaks of**
787 **spliceosomal crosslinking.**

788 (a) Crosslinking patterns of selected RBPs, as defined by cDNA starts of eCLIP or iCLIP in
789 the indicated cell lines. Crosslinking of each is regionally normalized to its average
790 crosslinking over -100..50 nt region relative to 3'ss in order to most clearly allow
791 comparisons between the relative positions of peaks for different RBPs. All 3'ss that
792 contain BPs within 17..23 nt upstream of the exon are chosen, and crosslinking is plotted
793 in the region -40..10 nt relative to 3'ss, and -40..10 nt relative to BPs.

794 (b) Same as (a), but for all 3'ss that contain BPs within 24..39 nt upstream of the exon.

795 (c) Same as (a), but for all 3'ss that contain BPs within 40..65 nt upstream of the exon.

796

797 **Supplementary Fig. 7 | Relation of BP position and consensus score to binding of**
798 **splicing factors.**

799 (b) Heatmaps depicting the normalized crosslinking of RBPs in peak regions around 10
800 groups of BPs that were categorized according to the distance of BPs from 3'ss.
801 Crosslinks were derived as cDNA starts from eCLIP of K562 cells.

802 (b) Heatmaps depicting the normalized crosslinking of RBPs in peak regions around 10
803 groups of BPs that were categorized according to the computational scores that define
804 BP strength. Crosslinks were derived as cDNA starts from eCLIP of K562 cells.

805 (c) BPs were divided into 10 quantiles based on their sequence consensus score, as
806 determined previously[11]. The median score of each quantile is shown on the x-axis. The
807 4,410 BPs chosen for this analysis satisfied two criteria: 1) They were located 23-28 nt
808 away from intron-exon junction, and 2) they contained a total of at least 30 crosslink
809 events of SF3 (SF3B4−K562−eCLIP, SF3B4−HepG2−eCLIP and SF3A3−HepG2−eCLIP) in
810 the region 35-10 nt upstream of BPs and U2AF (U2AF2−HepG2−eCLIP,
811 U2AF2−K562−eCLIP and U2AF1−K562−eCLIP) in the region 5-25 nt downstream of BPs
812 (the peak binding region of these RBPs). The y-axis shows the ratio in binding of SF3
813 relative to U2AF factors (data and positions as in the preceding sentence). P-values for
814 the indicated comparisons were calculated by the pairwise Wilcoxon Rank Sum test.
815 Box-plot elements are defined by center line, median; box limits, upper and lower
816 quartiles; and whiskers, 1.5x interquartile range.

817 (d) BPs were divided into 10 quantiles as in (c). The % of Ys (C or T) in the region 1-21
818 nt downstream of BPs is shown on the y-axis. Box-plot elements are defined by center
819 line, median; box limits, upper and lower quartiles; and whiskers, 1.5x interquartile
820 range.

821
822

823 **Methods:**

824 **Data and statistics**

825 The spliceosome iCLIP data have been deposited on EBI ArrayExpress under the
826 accession number E-MTAB-6950. These and published datasets referenced throughout
827 this study are listed for convenience in Supplementary Table 7, including accession
828 details. All statistical analyses were performed in the R software environment (version
829 3.1.3 and 3.3.2, https://www.r-project.org).

830 **Code availability**

831 The code to identify BPs from spliceosome iCLIP reads is publicly available at the GitHub
832 repository (https://github.com/nebo56/branch-point-detection-2).

833 **Preparation of Cal51 cells for iCLIP**

834 Cal51 breast adenocarcinoma cells were prepared as described previously[4]. Briefly, cells
835 were cultured in Dulbecco's Modified Eagle Medium (DMEM, ThermoFisher) with 10%
836 fetal calf serum (FCS, ThermoFisher) and 1× penicillin-streptomycin (P/S,
837 ThermoFisher). For siRNA-mediated depletion of PRPF8, Cal51 cells were transfected
838 with DharmaFECT1 (Dharmafect) with 25 nM siRNA targeting human *PRPF8*.
839 Transfected cells were harvested 54 hrs later, exposed to UV-C light and used for iCLIP
840 as described below. For collection of samples from different stages of the cell cycle,
841 Cal51 cells were synchronized in G1/S by standard double thymidine block. Briefly, cells
842 were treated with 1.5 mM thymidine for 8 hrs, washed and released for 8 hrs, then
843 treated again with thymidine for a further 8 hrs. Cells were also collected 3 hrs (S-
844 phase) and 7 hrs (G2) after release from the thymidine block.

845 ***In vitro* splicing**

846 For *in vitro* splicing reactions, a *C6orf10* minigene construct containing exon 8 and 9 and
847 150 nt of the intron around both splice sites was produced (Fig. 2b). The minigene
848 plasmid was linearized and transcribed *in vitro* using T7 polymerase with ^{32}P-UTP. The
849 transcribed RNA was then subjected to *in vitro* splicing reactions using HeLa nuclear
850 extract. HeLa nuclear extract was depleted of endogenous ATP by pre-incubation and,
851 for each reaction, 10 ng of RNA was incubated with 60% HeLa nuclear extract at 30°C
852 with or without additional 0.5 mM ATP for 1 h in a 20 µl reaction. Afterwards, the
853 reaction mixture was UV-crosslinked at 100 mJ/cm^2 and stored at -80°C until further
854 use. To visualize the splicing reaction products, proteinase K was added to the reaction
855 mixture for 30 min at 37°C. The resulting RNA was phenol-extracted, precipitated and
856 subjected to gel electrophoresis on a 5% polyacrylamide-urea gel.

857 **Spliceosome iCLIP protocol**

858 For each experiment, three biological replicate samples of cDNA libraries were prepared
859 (Supplementary Tables 2 and 3). The iCLIP method was done as previously described[10],
860 with the following modifications. Crosslinked cells or tissue were dissociated in the lysis
861 buffer according to the stringency conditions (stringent, medium, mild; Supplementary

862 Table 1) followed by sonication, low RNase I (AM2295, 100 U/µl, ThermoFisher)
863 digestion and centrifugation. RNase at low concentration ensured that cDNAs are
864 optimal size for comprehensive crosslink determination[14]. For denaturing, high-
865 stringency experiment[10], M2 anti-Flag antibody (Sigma) was used against the 3×Flag-
866 SmB protein that had been stably integrated into HEK-293 FlpIn cells (Supplementary
867 Fig. 1c). 6M Urea buffer was first used to lyse cell pellets, before being diluted down 1:9
868 with a Tween-20 containing IP buffer to allow for immuno-purification without
869 denaturing of the M2 anti-Flag antibody, and then proceeded as described previously[14].

870 Mouse brain tissue was used for initial experiments under mild and medium stringency
871 conditions (Supplementary Fig. 1e), HeLa nuclear extract was used for *in vitro* splicing
872 reactions (Supplementary Fig. 2c), and Cal51 cells were then used for all remaining
873 experiments, since they have proven well-suited to understand the impact of
874 spliceosomal perturbations on cell cycle[4]. For SmB/B' immunopurification under
875 medium and mild conditions, anti-SmB/B' antibodies 12F5 (sc-130670, Santa Cruz
876 Biotechnology) or 18F6 (as hybridoma supernatant, generated as described previously[9])
877 were used, which are different clones from the same immunization. These antibodies
878 behave identically under immunopurification conditions (Supplementary Fig. 1d). For
879 spliceosome iCLIP from mouse brain and *in vitro* splicing reactions, lysates were
880 incubated with 50 µl monoclonal anti-SmB/B' antibody 18F6, and for experiments from
881 Cal51 cells, 12F5 anti-SmB/B' antibody (Santa Cruz) was used. The antibody was pre-
882 conjugated to 100 µl protein G Dynabeads (ThermoFisher) and rotated at 4°C followed
883 by washing. As described previously, following immunopurification, RNA 3' end
884 dephosphorylation, ligation of the linker 5'-rAppAGATCGGAAGAGCGGTTCAG/ddC/-3' to
885 the 3' end and 5' end radiolabeling protein-RNA complexes were size-separated by SDS-
886 PAGE and transferred onto nitrocellulose membrane. The regions corresponding to 28-
887 180 kDa were excised from the membrane in order to isolate the bound RNA by
888 proteinase K treatment. RNAs were reverse-transcribed in all experiments using
889 SuperScript III reverse transcriptase at U/µl (ThermoFisher) and custom indexed
890 primers (Table S2). Resulting cDNAs were subjected to electrophoresis on a 6% TBE-
891 urea gel (ThermoFisher) for size selection. Purified cDNAs were circularized, linearized
892 and amplified for high-throughput sequencing.

893 Identification of protein crosslink sites around splice sites, in particular at the peaks
894 4/5, was most efficient under the mild purification condition (Supplementary Fig. 2a).
895 This condition was therefore used for analysis of spliceosomal assembly upon PRPF8
896 knockdown in Cal51 cells (Fig. 2a), and in the *in vitro* splicing reactions in HeLa nuclear
897 extract (Fig. 2b). For the identification of BPs, we additionally used the medium
898 condition, since it increases the frequency of cDNAs truncating at peak B
899 (Supplementary Fig. 2a). For this purpose, spliceosome iCLIP was performed under
900 medium purification conditions from Cal51 cells synchronized in G1, S and G2 phase. To
901 maximise cDNA coverage, data from all synchronized cells was merged with the control
902 Cal51 cells under mild condition for BP identification.

903 **Mapping of Sm iCLIP reads**

904 We used mm9/NCBI37 and hg19/GRCh37 genome versions and Ensembl 75 gene
905 annotation. Experimental and random barcode sequences of iCLIP sequenced reads
906 were removed prior to mapping (Supplementary Table 2). We mapped the cDNAs to the
907 genome with Bowtie 0.12.7 program using the parameters (-v 2 -m 1 -a --best --strata).
908 The first 9 nt of the sequenced reads contain the experimental barcode to separate
909 experimental replicates, and the random barcode, the latter of which allows to avoid
910 artefacts caused by variable PCR amplification of different cDNAs[8]. We used these
911 random barcodes to quantify the number of unique cDNAs at each genomic position by
912 collapsing cDNAs with the same random barcode that mapped to the same starting
913 position to a single cDNA. For analysis of crosslinking to snRNAs, we allowed sequences
914 to map at up to 50 locations in the genome, but for all other analyses in the manuscript,
915 we only allowed sequence mapping to a single location in the genome. For spliceosome
916 iCLIP with the *C6orf10 in vitro* splicing substrate, sequence reads were first mapped to
917 the unspliced substrates and the remaining reads were mapped to the spliced substrate
918 allowing no mismatches. The nucleotide preceding the iCLIP cDNAs was used to define
919 the crosslink sites.

920 **Mapping of eCLIP reads**

921 For eCLIP sequencing data for all RBPs, we used GENCODE (GRCh38.p7) genome
922 assembly and the STAR alignment (version 2.4.2a) using the following parameters from
923 ENCODE pipeline: STAR --runThreadN 8 --runMode alignReads --genomeDir GRCh38
924 Gencode v25 --genomeLoad LoadAndKeep --readFilesIn read1, read2, --
925 readFilesCommand zcat --outSAMunmapped Within –outFilterMultimapNmax 1 --
926 outFilterMultimapScoreRange 1 --outSAMattributes All --outSAMtype BAM Unsorted –
927 outFilterType BySJout --outFilterScoreMin 10 --alignEndsType EndToEnd --
928 outFileNamePrefix outfile.

929 For the PCR duplicates removal, we used a python script 'barcode collapse pe.py'
930 available on GitHub (https://github.com/YeoLab/gscripts/releases/tag/1.0), which is
931 part of the ENCODE eCLIP pipeline
932 (https://www.encodeproject.org/pipelines/ENCPL357ADL/).

933 **Normalization of crosslink positions for their visualization in the form of RNA**
934 **maps**

935 RNA maps were produced by summarizing the cDNA counts at each nucleotide using the
936 previously developed RNA maps pipeline [14,29] relative to exon/intron and intron/exon
937 boundaries and BPs on pre-mRNAs. The definition of intronic start and end positions
938 was based on Ensembl version 75. Only introns longer than 300 nt were used to draw
939 RNA maps in order to avoid detection of any RBPs that recognize 5'ss of introns.

940 In cases where we wished to compare the relative positions of crosslinking peaks
941 between RBPs, we regionally normalized the summarized crosslinking of each RBP
942 relative to the average crosslinking of the same RBP across the region 100 nt upstream

943 and 50 nt downstream of the evaluated splice sites or branchpoints. Normalized values
944 were then used to visualize the crosslinking in the form of RNA maps (Fig. 2,
945 Supplementary Fig. 5 and 6).

946 To assess the role of BP characteristics on spliceosomal RBP assembly (Fig. 4, 6 and 7),
947 we only examined the introns containing the 31,167 BPs that were identified both
948 computationally and by iCLIP, which are likely the most reliable. We divided BPs into 10
949 categories based on BP position or score, and then normalized the summarized
950 crosslinking of each RBP in each of the 10 BP categories relative to the average
951 crosslinking of the same RBP across the region 100 nt upstream and 50 nt downstream
952 of all the 31,167 evaluated BPs.

953 **Identification and comparison of branchpoints (BPs)**

954 It has been shown that the spliceosomal C complexes harbor a salt-resistant RNP core
955 containing U2, U5 and U6 snRNAs as well as the splicing intermediates including lariats
956 that withstand treatment with 1M NaCl, whereas the spliceosomal B complexes were
957 more likely dissociated under high-salt conditions[16]. This could explain why the medium
958 purification condition is more suited than the mild condition to enrich for lariat cDNAs
959 truncating at position B (Supplementary Fig. 2a). It is conceivable that the medium
960 spliceosome iCLIP condition most strongly enriches spliceosomal C complexes, which
961 are most effective for lariat detection. In contrast, the mild condition is expected to
962 enrich additional B complexes that contain large amounts of SF3 components and have
963 low proportion of lariats, in agreement with the strong enrichment of peaks 4 and 5
964 (Supplementary Fig. 2a). To identify the maximal diversity of BPs, we therefore pooled
965 spliceosome iCLIP data produced under mild and medium purification conditions from
966 Cal51 cells.

967 The first step to identify BPs used the spliceosome iCLIP reads that ended precisely at
968 the ends of introns (we considered only introns that end in AG dinucleotide) after
969 removal of the 3' adapter. We noticed that these reads had an 3.5× increased frequency
970 of mismatches on the A as the first nucleotide compared to remaining iCLIP reads
971 (Supplementary Fig. 3a), indicating that these mismatches may have resulted from
972 truncation at the three-way-junction formed at the BP (Fig. 2c). We therefore trimmed
973 the first nucleotide from the read if it contained a mismatch at the first position that
974 corresponded to a genomic adenosine. We then used spliceosome iCLIP from Cal51 cells
975 to identify all reads that ended precisely at the ends of introns and defined the position
976 where these reads started and assessed the random barcode nucleotides that are
977 present at the beginning of each iCLIP read to count the number of unique cDNAs at
978 each position. The nucleotide preceding the read start corresponds to the position
979 where cDNAs truncated during the reverse transcription, and we selected the genomic A
980 that had the highest number of truncated cDNAs as the candidate BP. If two positions
981 with equal number of cDNAs were found, we selected the one closer to the 3'ss. For all
982 branchpoint analyses, we only assessed protein-coding genes with FPKM>10 in the
983 RNA-seq data, which identified 35,056 BP positions.

984 In the second step of analysis, we considered all cDNAs (regardless of where they
985 ended), but including trimming of the first nucleotide if there was a mismatch with the
986 genomic A. We then overlapped cDNA truncation sites with computationally predicted
987 BPs in the last 100 nt of intron[17]. If this analysis identified a position with a higher cDNA
988 count than the initial analysis (or if the initial analysis didn't identify any BP in the same
989 intron), then the newly identified position was assigned as the BP. For introns where no
990 BP was identified by either the first or second step in the analysis, we assessed
991 computationally predicted BPs located further than 100 nt from the 3'ss, and if any of
992 these overlapped with a truncating cDNA, we assigned the position closest to the 3'ss as
993 the BP. Together, this identified 50,812 BPs in genes with FPKM>10. The coordinates of
994 these BPs were used for analyses presented in the Figures 4-7. We additionally
995 identified 13,496 BPs in introns of lowly expressed genes, but these were not used for
996 any further analyses.

997 We also attempted to use truncated cDNAs from PRPF8 eCLIP for discovery of BPs, but
998 found that the number of cDNAs overlapping with intron ends was much smaller than in
999 spliceosome iCLIP, and was insufficient for BP discovery. This is most likely because the
1000 high amount of non-specific background signal in PRPF8 eCLIP, which leads to a lower
1001 proportion of cDNAs that align to the BPs.

1002 Bedtools Intersect command using option –u was used to compare BP coordinates from
1003 spliceosome iCLIP to the BPs identified in previous studies. We restricted this
1004 comparison to introns where BPs were detected by all three datasets (iCLIP, RNA-seq
1005 and computational prediction).

1006 To define a single 'computational BP' per intron, the BP positions computationally
1007 predicted for each intron in hg19 were obtained from11:
1008 http://bejerano.stanford.edu/labranchor/, and top scoring BP in each intron was use.
1009 To define a single 'RNA-seq BP' per intron, we used the BP with most lariat-spanning
1010 reads in each intron.

1011 **Analysis of pairing probability**

1012 Computational predictions of the secondary structure were performed by RNAfold
1013 function from Vienna Package (https://www.tbi.univie.ac.at/RNA/) with default
1014 parameters[28]. The RNAfold results are provided in a customized format, where brackets
1015 are representing the double stranded region on the RNA and dots are used for unpaired
1016 nucleotides. We measured the density of pairing probability by summing the paired
1017 positions into a single vector.

1018 **Identification of RBPs overlapping with spliceosomal peaks**

1019 For RBP enrichment in Fig. 4, we used the eCLIP data from the ENCODE consortium[15],
1020 together with available iCLIP experiments from our lab (which are all listed in[22]), to see
1021 if any of the proteins are enriched in the region of spliceosomal peaks. In total this

1022 included 157 eCLIP samples of 68 RBPs in the HepG2 cell line, and 89 RBPs in the K562
1023 cell, and iCLIP samples of 18 RBPs from different cell lines (Supplementary Table 5).
1024 Next, we intersected cDNA-starts from each sample to the -100 to +50 nt region relative
1025 to the 3'ss and used it as control for each of the following peaks: Peak 4 (-23 nt..-29 nt
1026 relative to BP), Peak 5 (-21 nt..-17 nt relative to BP), Peak B (-1 nt..1 nt relative to BP),
1027 Peak A (-1 nt..1 nt relative to 5'ss), Peak 6 (-11 nt..-10 nt relative to 3'ss), Peak 7 (-3 nt..-
1028 2 nt relative to 3'ss). The positions of these peaks were determined based on crosslink
1029 enrichments in spliceosome iCLIP.

Figure 1

A

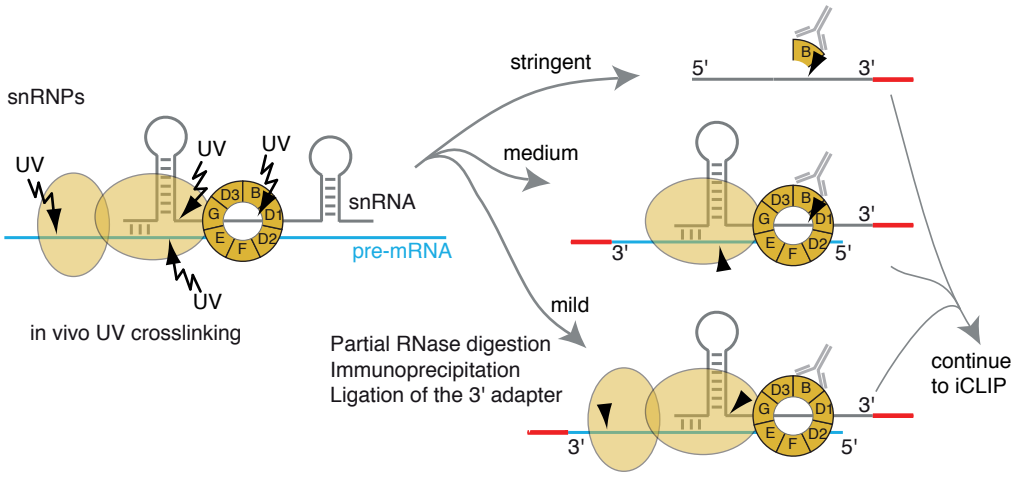
snRNPs
UV
UV
UV
UV
snRNA
pre-mRNA
in vivo UV crosslinking
stringent
medium
mild
5'
3'
3'
5'
3'
5'
3'
5'
Partial RNase digestion
Immunoprecipitation
Ligation of the 3' adapter
continue
to iCLIP

B

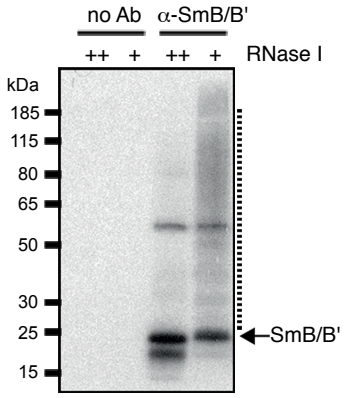
no Ab
α-SmB/B'
++ + ++ +
RNase I
kDa
185
115
80
65
50
30
25
15
SmB/B'

C

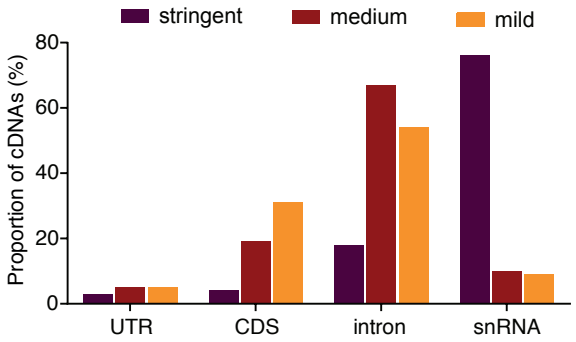
stringent
medium
mild
Proportion of cDNAs (%)
80
60
40
20
0
UTR
CDS
intron
snRNA

Figure 2

A

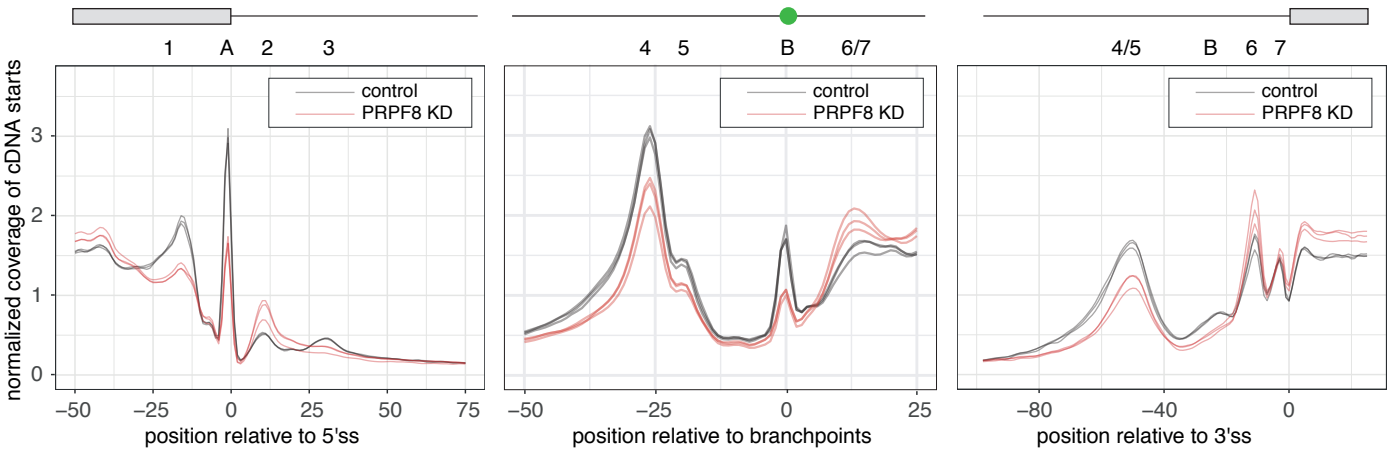
1
A
2
3
4
5
B
6/7
4/5
B
6
7
control
PRPF8 KD
normalized coverage of cDNA starts
position relative to 5'ss
position relative to branchpoints
position relative to 3'ss

B

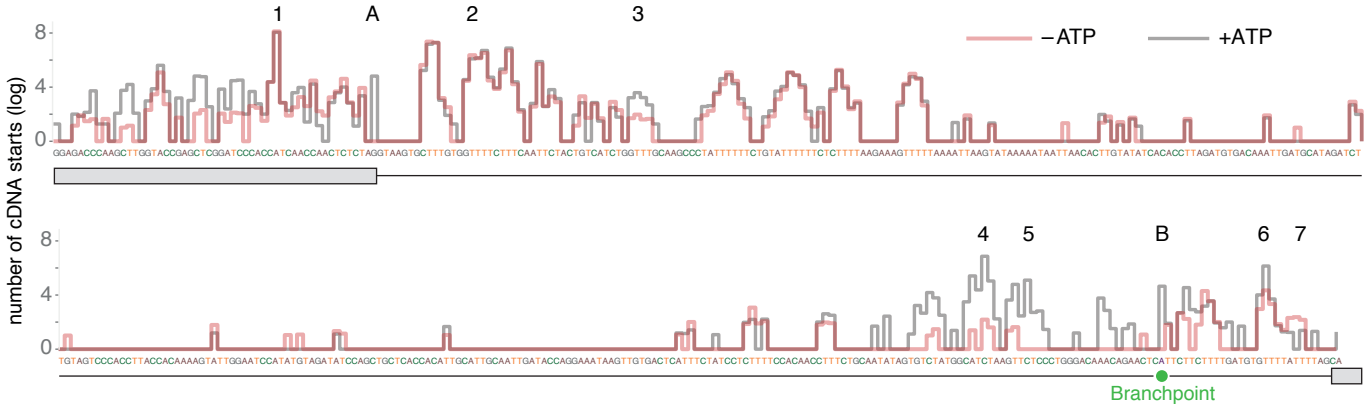
1
A
2
3
4
5
B
6
7
−ATP
+ATP
number of cDNA starts (log)
Branchpoint

C

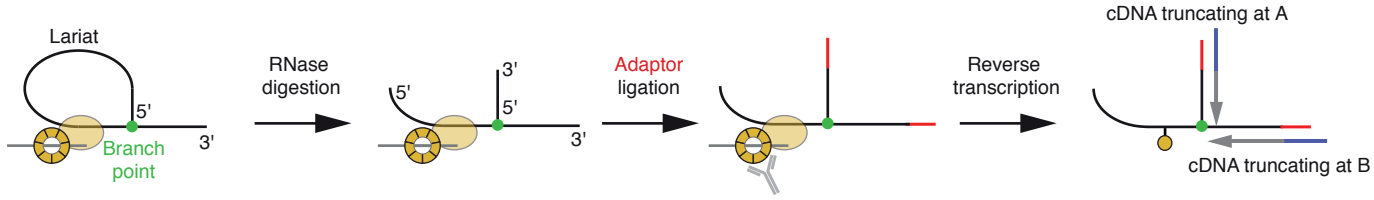
Lariat
5'
3'
Branch point
RNase digestion
Adaptor ligation
Reverse transcription
cDNA truncating at A
cDNA truncating at B

Figure 3

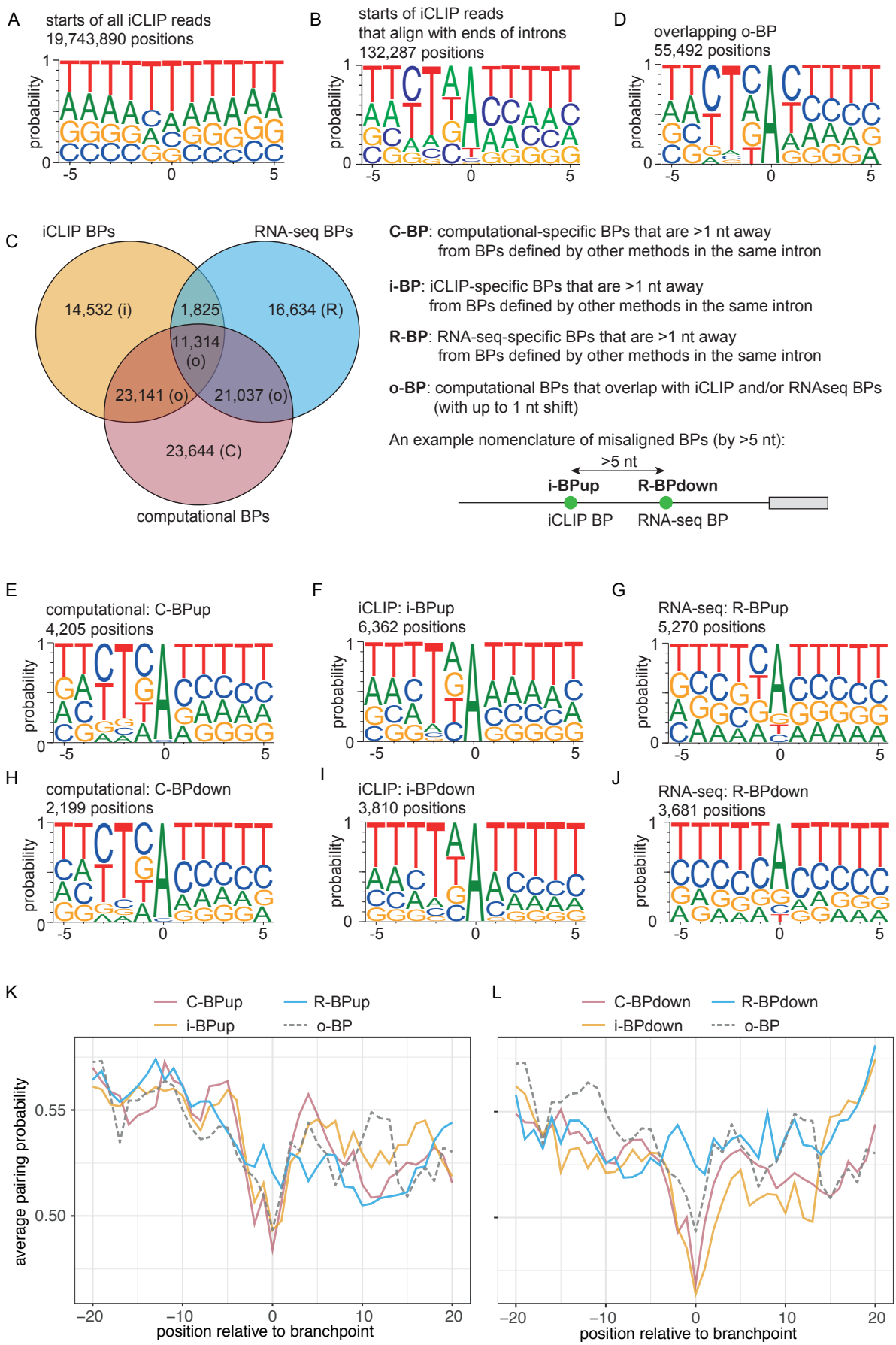
A
starts of all iCLIP reads
19,743,890 positions
B
starts of iCLIP reads
that align with ends of introns
132,287 positions
D
overlapping o-BP
55,492 positions
probability
C
iCLIP BPs
RNA-seq BPs
14,532 (i)
1,825
16,634 (R)
11,314
(o)
23,141 (o)
21,037 (o)
23,644 (C)
computational BPs
C-BP: computational-specific BPs that are >1 nt away
from BPs defined by other methods in the same intron
i-BP: iCLIP-specific BPs that are >1 nt away
from BPs defined by other methods in the same intron
R-BP: RNA-seq-specific BPs that are >1 nt away
from BPs defined by other methods in the same intron
o-BP: computational BPs that overlap with iCLIP and/or RNAseq BPs
(with up to 1 nt shift)
An example nomenclature of misaligned BPs (by >5 nt):
>5 nt
i-BPup
R-BPdown
iCLIP BP
RNA-seq BP
E
computational: C-BPup
4,205 positions
F
iCLIP: i-BPup
6,362 positions
G
RNA-seq: R-BPup
5,270 positions
H
computational: C-BPdown
2,199 positions
I
iCLIP: i-BPdown
3,810 positions
J
RNA-seq: R-BPdown
3,681 positions
K
C-BPup
R-BPup
i-BPup
o-BP
average pairing probability
position relative to branchpoint
L
C-BPdown
R-BPdown
i-BPdown
o-BP
position relative to branchpoint

Figure 4

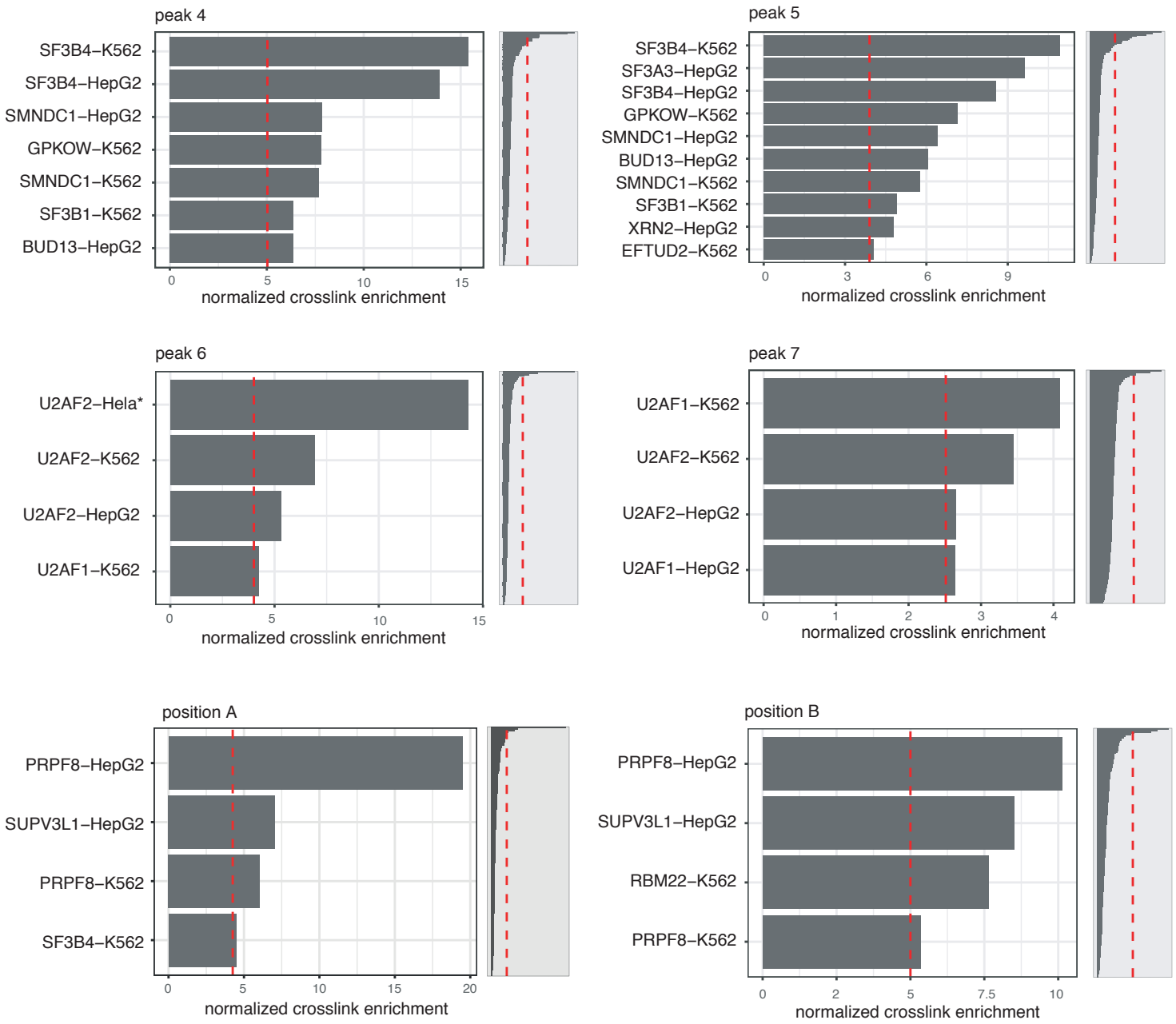
peak 4
SF3B4−K562
SF3B4−HepG2
SMNDC1−HepG2
GPKOW−K562
SMNDC1−K562
SF3B1−K562
BUD13−HepG2
0
5
10
15
normalized crosslink enrichment
peak 5
SF3B4−K562
SF3A3−HepG2
SF3B4−HepG2
GPKOW−K562
SMNDC1−HepG2
BUD13−HepG2
SMNDC1−K562
SF3B1−K562
XRN2−HepG2
EFTUD2−K562
0
3
6
9
normalized crosslink enrichment
peak 6
U2AF2−Hela*
U2AF2−K562
U2AF2−HepG2
U2AF1−K562
0
5
10
15
normalized crosslink enrichment
peak 7
U2AF1−K562
U2AF2−K562
U2AF2−HepG2
U2AF1−HepG2
0
1
2
3
4
normalized crosslink enrichment
position A
PRPF8−HepG2
SUPV3L1−HepG2
PRPF8−K562
SF3B4−K562
0
5
10
15
20
normalized crosslink enrichment
position B
PRPF8−HepG2
SUPV3L1−HepG2
RBM22−K562
PRPF8−K562
0
2
5
7.5
10
normalized crosslink enrichment

Figure 5

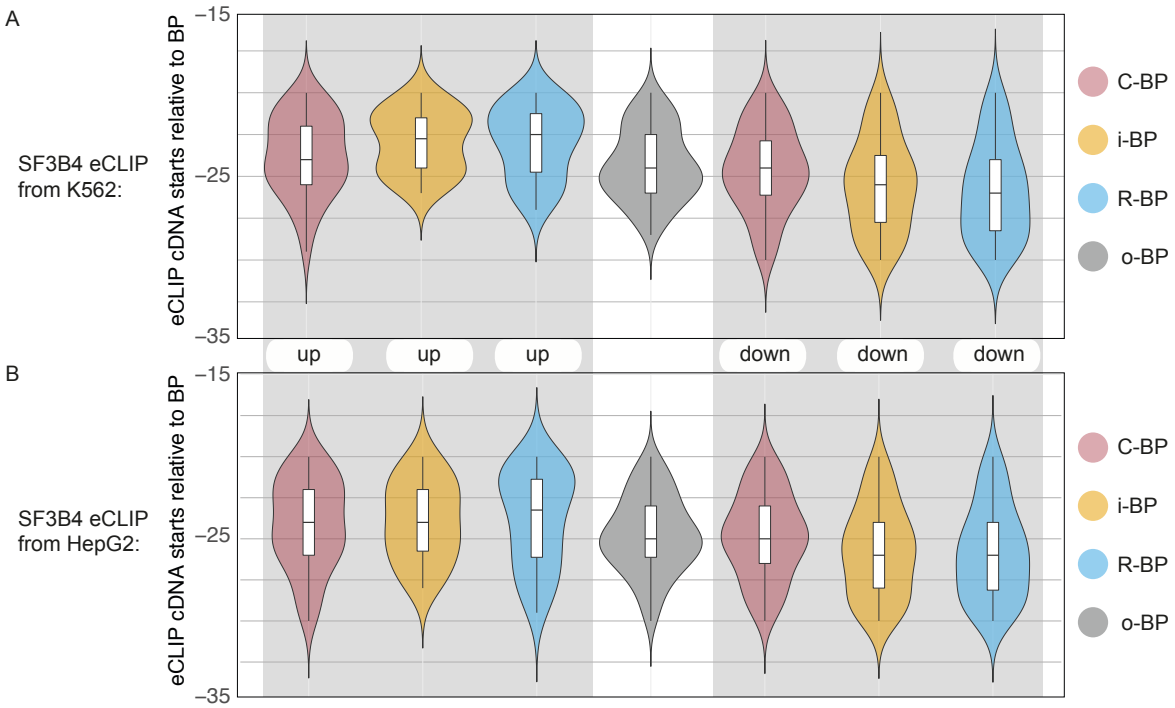
A
SF3B4 eCLIP
from K562:
eCLIP cDNA starts relative to BP
−15
−25
−35
up
up
up
down
down
down
C-BP
i-BP
R-BP
o-BP
B
SF3B4 eCLIP
from HepG2:
eCLIP cDNA starts relative to BP
−15
−25
−35
C-BP
i-BP
R-BP
o-BP

Figure 6

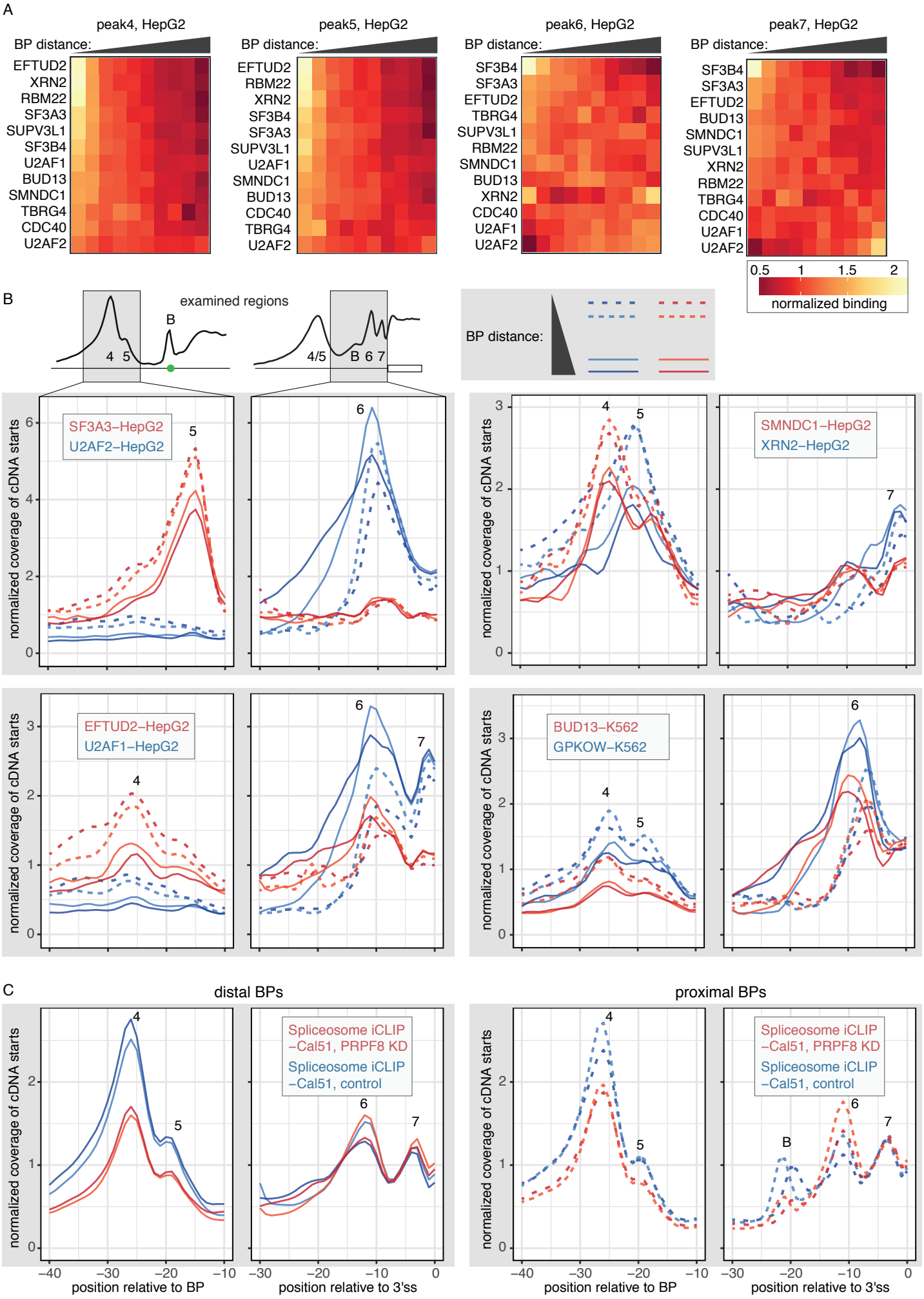
A
peak4, HepG2
BP distance:
EFTUD2
XRN2
RBM22
SF3A3
SUPV3L1
SF3B4
U2AF1
BUD13
SMNDC1
TBRG4
CDC40
U2AF2
peak5, HepG2
BP distance:
EFTUD2
RBM22
XRN2
SF3B4
SF3A3
SUPV3L1
U2AF1
SMNDC1
BUD13
CDC40
TBRG4
U2AF2
peak6, HepG2
BP distance:
SF3B4
SF3A3
EFTUD2
TBRG4
SUPV3L1
RBM22
SMNDC1
BUD13
XRN2
CDC40
U2AF1
U2AF2
peak7, HepG2
BP distance:
SF3B4
SF3A3
EFTUD2
BUD13
SMNDC1
SUPV3L1
XRN2
RBM22
TBRG4
CDC40
U2AF1
U2AF2
0.5
1
1.5
2
normalized binding
B
examined regions
4 5
B
4/5
B 6 7
BP distance:
normalized coverage of cDNA starts
SF3A3–HepG2
U2AF2–HepG2
SMNDC1–HepG2
XRN2–HepG2
EFTUD2–HepG2
U2AF1–HepG2
BUD13–K562
GPKOW–K562
C
distal BPs
proximal BPs
Spliceosome iCLIP
–Cal51, PRPF8 KD
Spliceosome iCLIP
–Cal51, control
position relative to BP
position relative to 3'ss

Figure 7

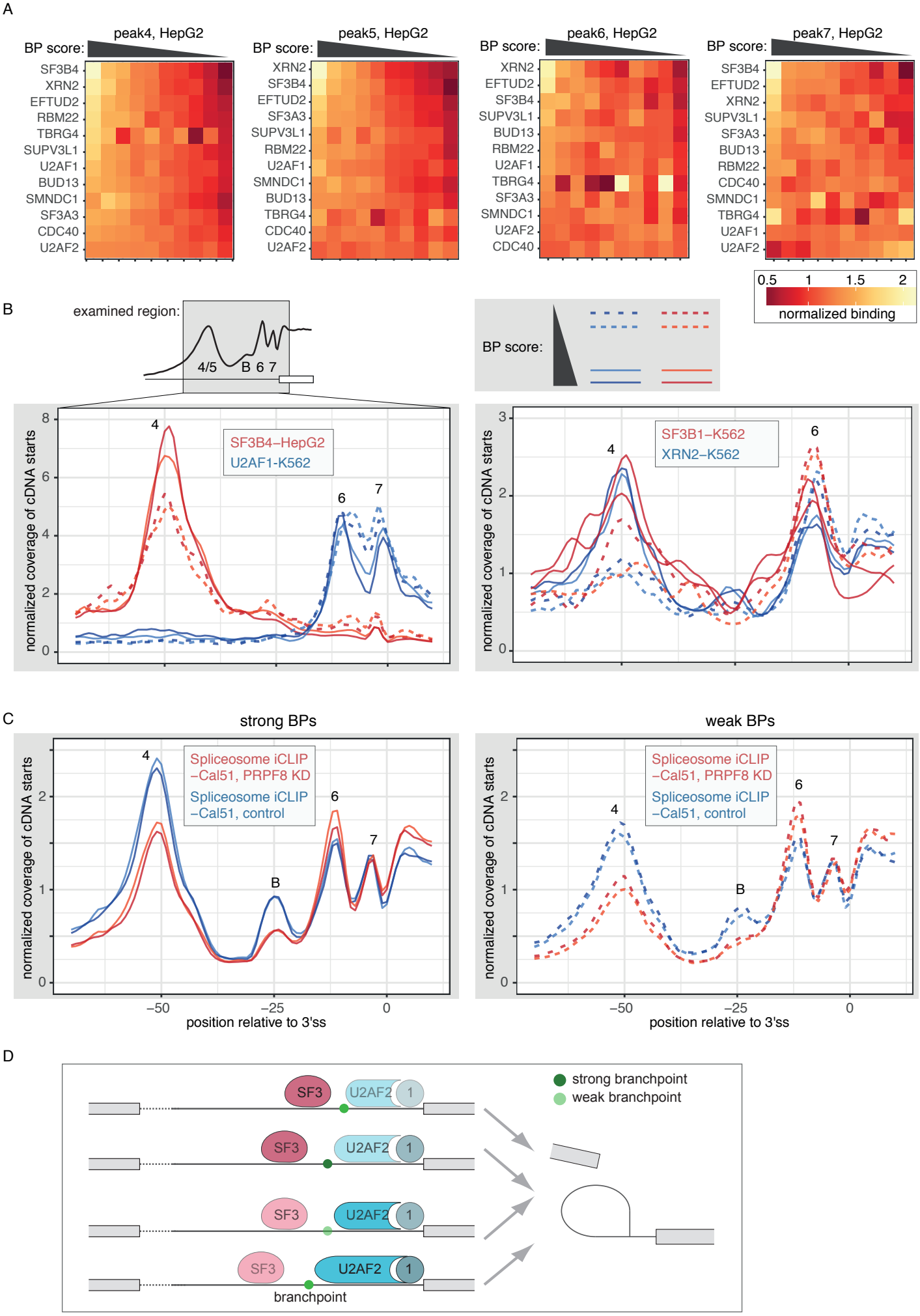
A
peak4, HepG2
peak5, HepG2
peak6, HepG2
peak7, HepG2
BP score:
SF3B4
XRN2
EFTUD2
RBM22
TBRG4
SUPV3L1
U2AF1
BUD13
SMNDC1
SF3A3
CDC40
U2AF2
0.5
1
1.5
2
normalized binding
B
examined region:
4/5
B 6 7
BP score:
SF3B4–HepG2
U2AF1-K562
SF3B1–K562
XRN2–K562
normalized coverage of cDNA starts
C
strong BPs
weak BPs
Spliceosome iCLIP
–Cal51, PRPF8 KD
Spliceosome iCLIP
–Cal51, control
position relative to 3'ss
D
SF3
U2AF2
1
strong branchpoint
weak branchpoint
branchpoint

Supplementary Figure 1

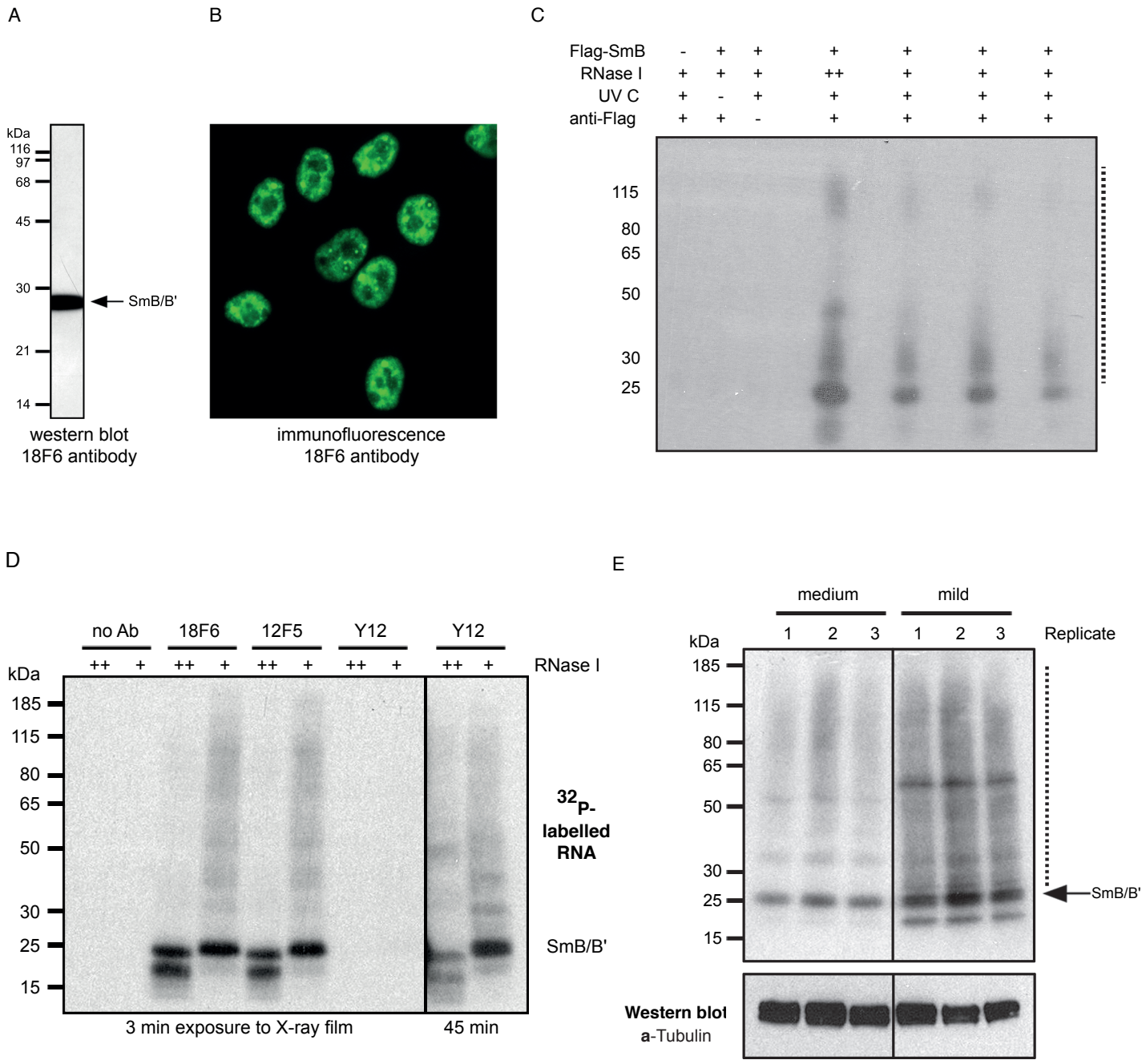

Supplementary Figure 2

A

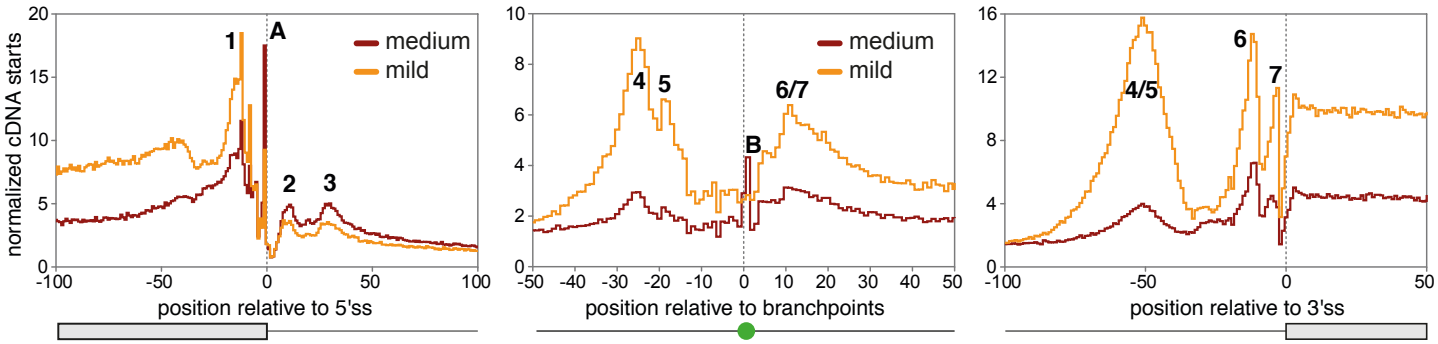

B

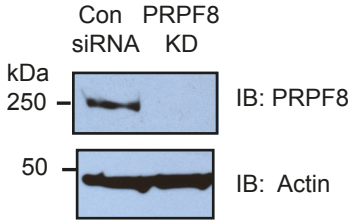

C

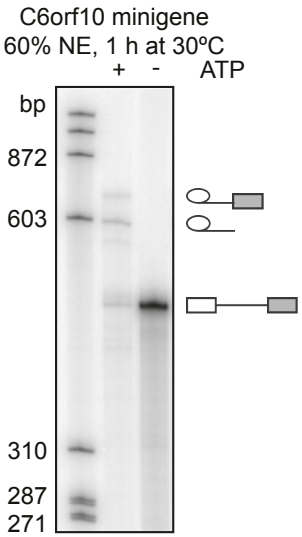

D

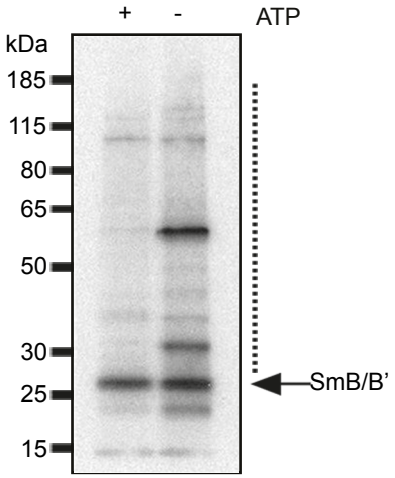

E

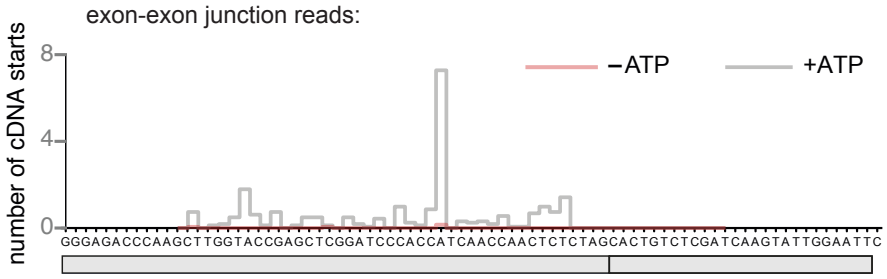

Supplementary Figure 3

A

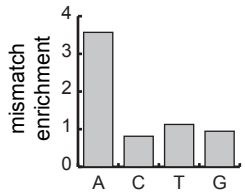

B

BP type	BP description	Number of BPs
overlapping	Top-scoring computational BP overlaps with iCLIP BP	31167
≤ 5nt	Top-scoring computational BP is ≤ 5nt from iCLIP BP	7787
> 5nt	Top-scoring computational BP is > 5nt from iCLIP BP	11858

C

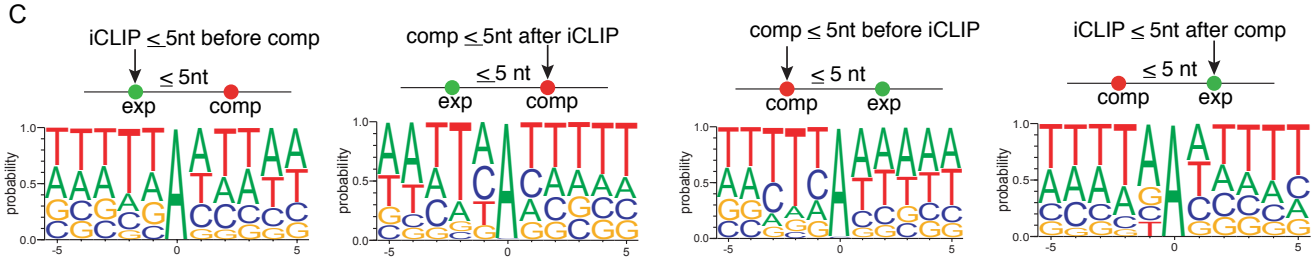

D

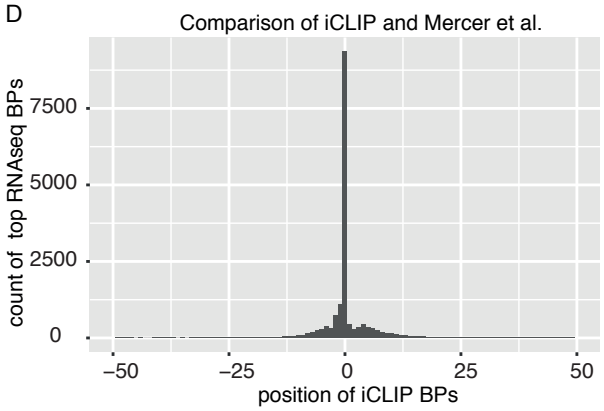

E

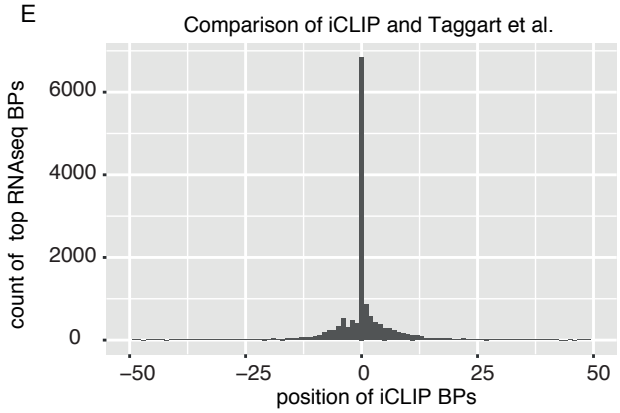

F

Study	BP positioning	Introns
Mercer et al.	overlapping with iCLIP BP	9348
	≤ 5nt of iCLIP BP	4604
	> 5nt of iCLIP BP	3095

G

Study	BP positioning	Introns
Taggart et al.	overlapping with iCLIP BP	6853
	≤ 5nt of iCLIP BP	4553
	> 5nt of iCLIP BP	3766

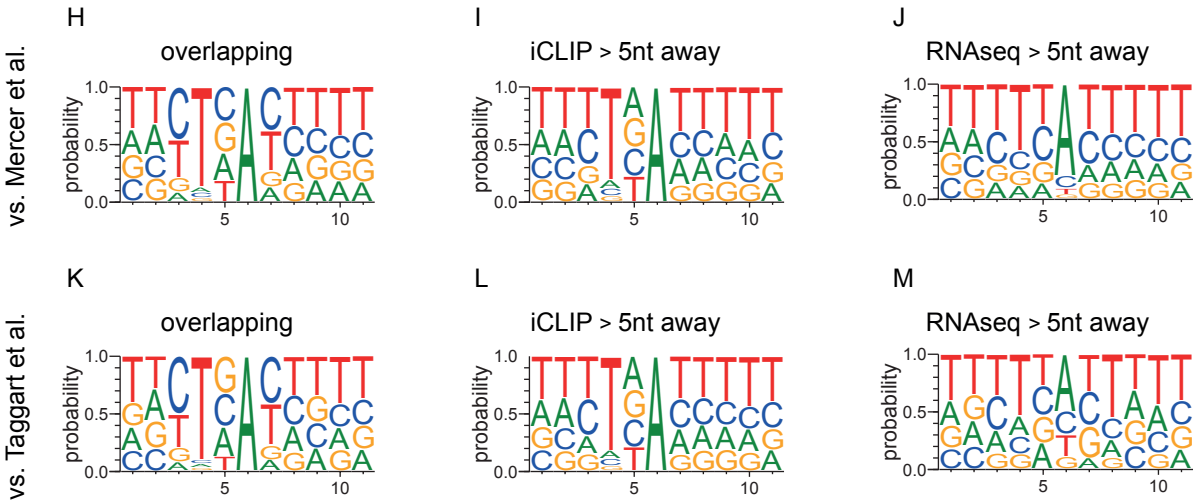

Supplementary Figure 4

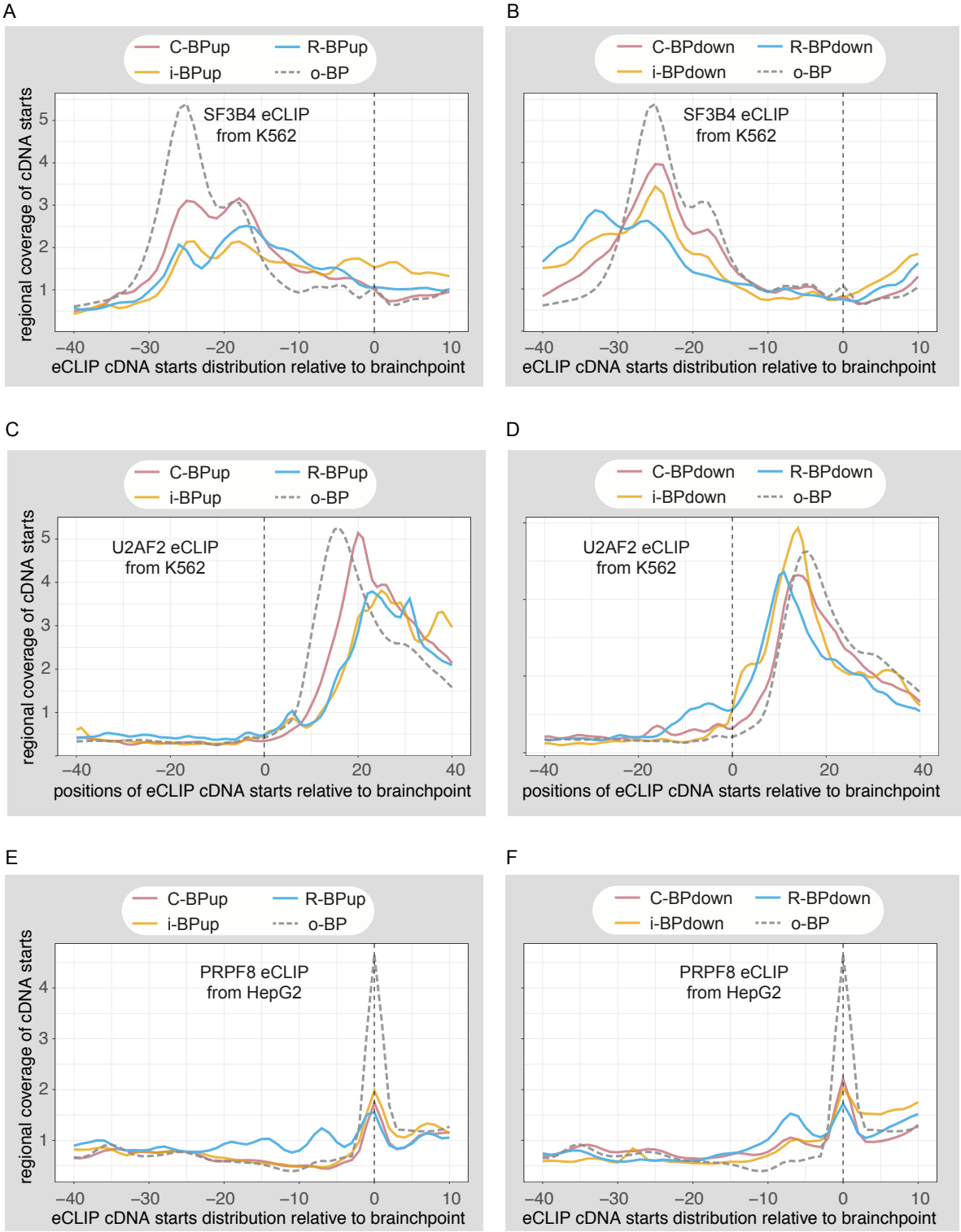

Supplementary Figure 5

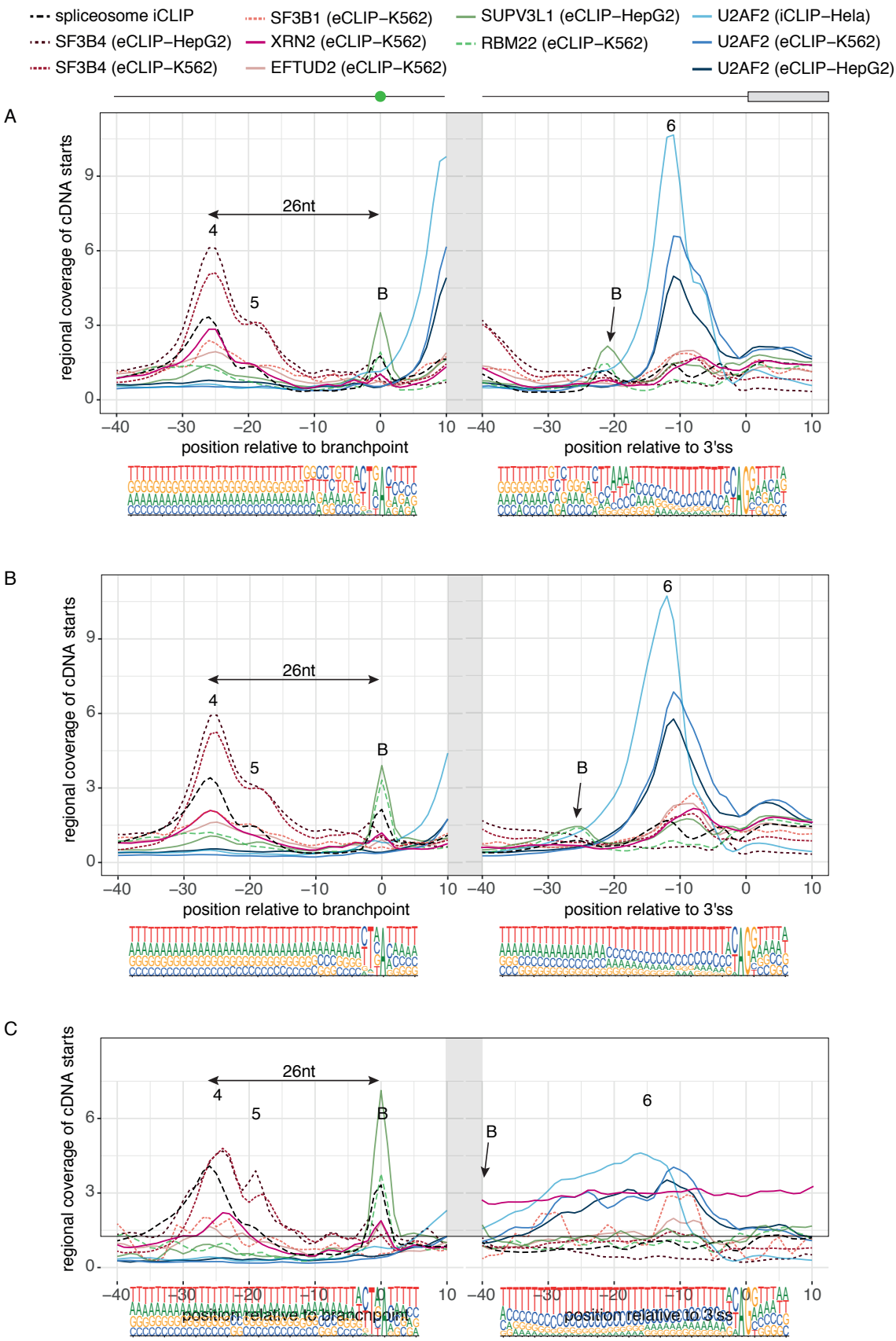

Supplementary Figure 6

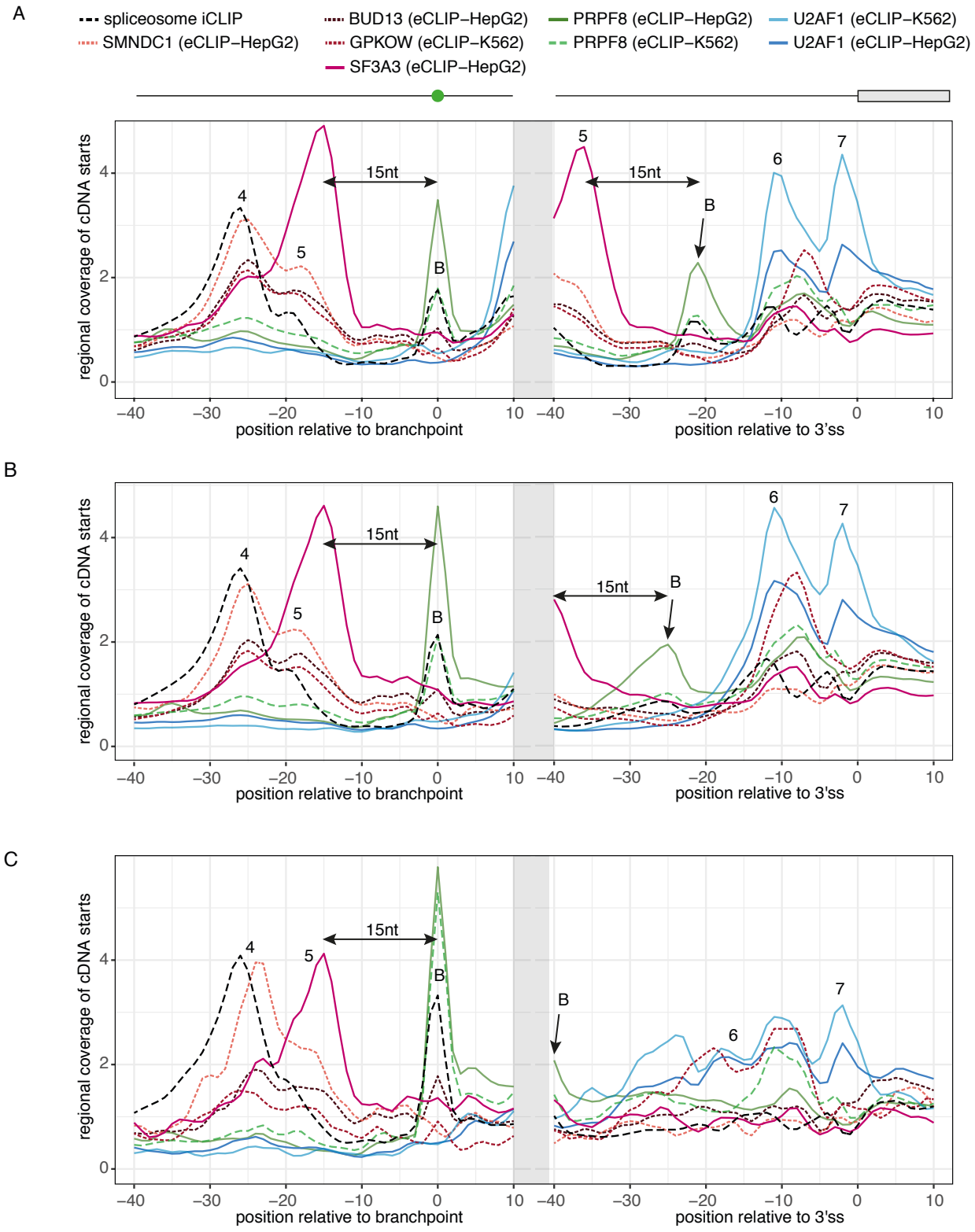
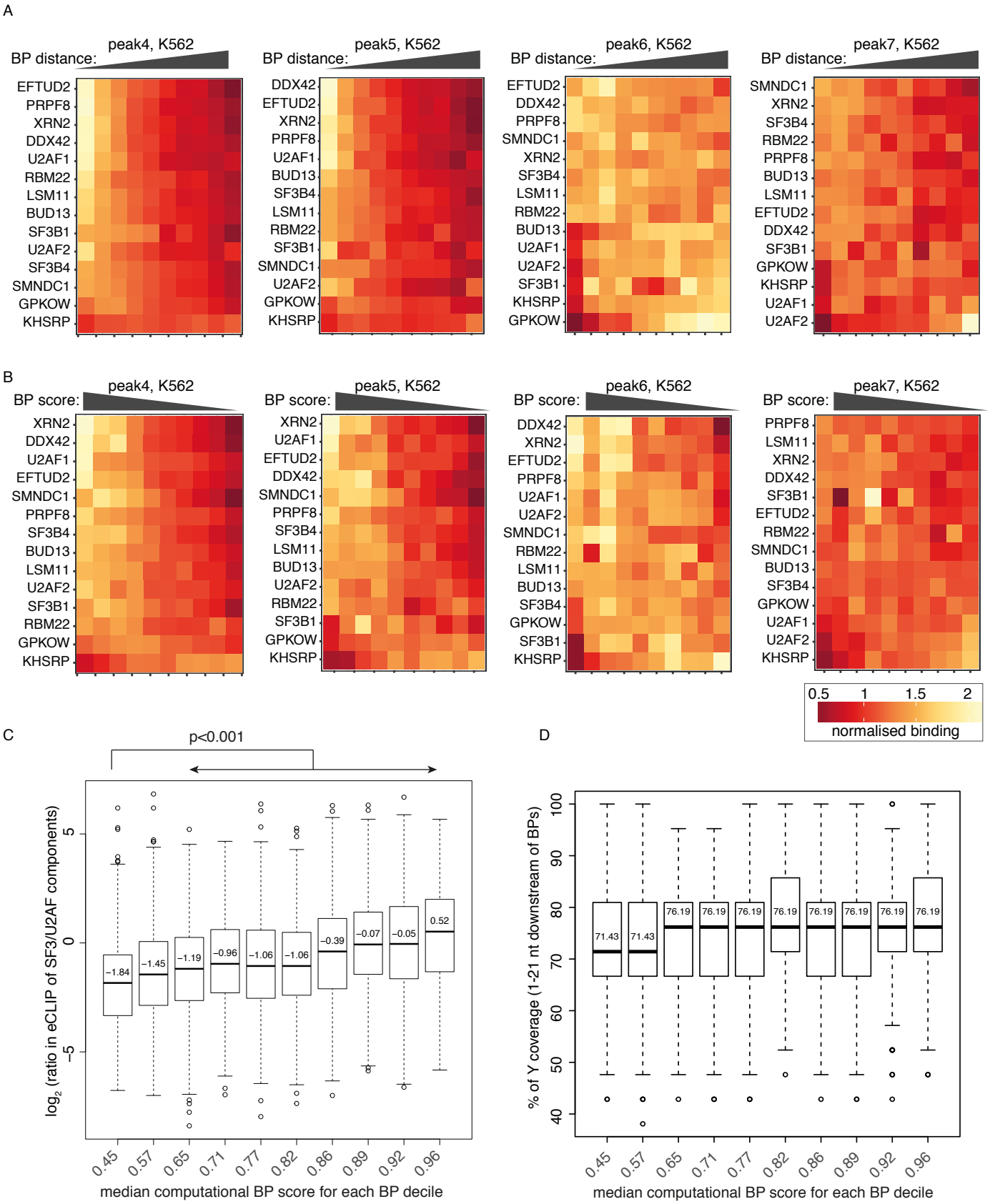
Supplementary Figure 7